

What Controls the Duration of El Niño and La Niña Events?

XIAN WU, YUKO M. OKUMURA, AND PEDRO N. DIÑEZIO

Institute for Geophysics, Jackson School of Geosciences, The University of Texas at Austin, Austin, Texas


(Manuscript received 10 October 2018, in final form 17 June 2019)

ABSTRACT

The temporal evolution of El Niño and La Niña varies greatly from event to event. To understand the dynamical processes controlling the duration of El Niño and La Niña events, a suite of observational data and a long control simulation of the Community Earth System Model, version 1, are analyzed. Both observational and model analyses show that the duration of El Niño is strongly affected by the timing of onset. El Niño events that develop early tend to terminate quickly after the mature phase because of the early arrival of delayed negative oceanic feedback and fast adjustments of the tropical Atlantic and Indian Oceans to the tropical Pacific Ocean warming. The duration of La Niña events is, on the other hand, strongly influenced by the amplitude of preceding warm events. La Niña events preceded by a strong warm event tend to persist into the second year because of large initial discharge of the equatorial oceanic heat content and delayed adjustments of the tropical Atlantic and Indian Oceans to the tropical Pacific cooling. For both El Niño and La Niña, the interbasin sea surface temperature (SST) adjustments reduce the anomalous SST gradient toward the tropical Pacific and weaken surface wind anomalies over the western equatorial Pacific, hastening the event termination. Other factors external to the dynamics of El Niño–Southern Oscillation, such as coupled variability in the tropical Atlantic and Indian Oceans and atmospheric variability over the North Pacific, also contribute to the diversity of event duration.

1. Introduction

El Niño–Southern Oscillation (ENSO) is the dominant mode of interannual climate variability and causes episodic warming (El Niño) and cooling (La Niña) of the tropical Pacific Ocean (e.g., Wallace et al. 1998; Neelin et al. 1998; Wang and Picaut 2004; Chang et al. 2006). Warm and cold ENSO events tend to last approximately 1–2 years and recur every 3–8 years. The ENSO drives atmospheric teleconnections that affect weather patterns, ecosystems, and economies around the world (e.g., Trenberth et al. 1998; Alexander et al. 2002). In particular, long-lasting ENSO events can exacerbate the climate impacts and cause significant hazards to our society (e.g., Hoerling and Kumar 2003; Okumura et al. 2017b). Thus, it is important to understand and predict the occurrence and evolution of individual ENSO events.

 Supplemental information related to this paper is available at the Journals Online website: <https://doi.org/10.1175/JCLI-D-18-0681.s1>.

Corresponding author: Xian Wu, xianwu0403@utexas.edu

The principal mechanism of ENSO is the positive ocean–atmosphere feedback originally proposed by Bjerknes (1969): an initial warm sea surface temperature (SST) anomaly in the eastern equatorial Pacific decreases the westward SST gradient and weakens the equatorial easterly winds, which in turn deepen the thermocline and reduce upwelling in the eastern equatorial Pacific, further amplifying the initial warming. This positive Bjerknes feedback also works for a cold event in the equatorial Pacific. The turnabout between El Niño and La Niña, on the other hand, is brought about by slow dynamical adjustments of the tropical ocean. For example, in the delayed oscillator theory, surface wind anomalies associated with El Niño and La Niña force oceanic equatorial Rossby waves, which reflect at the western boundary as equatorial Kelvin waves and reverse the thermocline anomalies in the eastern equatorial Pacific (Suarez and Schopf 1988; Battisti and Hirst 1989). Schneider et al. (1995) and Kirtman (1997) suggest that slower off-equatorial Rossby waves forced by wind stress curl anomalies play a more important role in the observed periodicity of ENSO. The Kelvin waves providing negative feedback may also be forced directly by surface wind changes over the far western equatorial

DOI: 10.1175/JCLI-D-18-0681.1

© 2019 American Meteorological Society. For information regarding reuse of this content and general copyright information, consult the [AMS Copyright Policy](#) (www.ametsoc.org/PUBSReuseLicenses).

Pacific (Weisberg and Wang 1997). The recharge oscillator theory, in contrast, emphasizes the role of basin-wide discharge/recharge of the equatorial oceanic heat content due to Sverdrup transport driven by surface wind anomalies without explicit equatorial wave propagation (Jin 1997).

Observed El Niño and La Niña events, however, significantly deviate from symmetric and regular oscillation explained by these linear ENSO theories. For instance, SST anomalies in the eastern equatorial Pacific are larger in magnitude for El Niño than La Niña (Burgers and Stephenson 1999). The associated atmospheric deep convection anomalies are displaced eastward during El Niño relative to La Niña (Hoerling et al. 1997) because of the nonlinear dependency of the atmospheric deep convection on SSTs (e.g., Gadgil et al. 1984; Graham and Barnett 1987). In addition to the amplitude and spatial pattern, the asymmetry in the duration of El Niño and La Niña has also been noted by a number of previous studies (Kessler 2002; Larkin and Harrison 2002; McPhaden and Zhang 2009; Ohba and Ueda 2009; Okumura and Deser 2010; Wu et al. 2010). Both El Niño and La Niña events usually develop in late boreal spring–summer and peak near the end of the calendar year. After the mature phase, El Niño tends to decay rapidly by next summer, but about one-half of La Niña events linger through the following year and reintensify in the subsequent winter.

Various mechanisms have been proposed to explain the asymmetric duration of El Niño and La Niña, emphasizing the nonlinearities in the tropical ocean–atmosphere system. Regarding the atmospheric nonlinearities, Okumura et al. (2011) suggest that the eastward shift of atmospheric deep convection anomalies during El Niño relative to La Niña makes surface winds over the western equatorial Pacific more susceptible to delayed basinwide warming of the Indian Ocean SST, which acts to terminate El Niño (Annamalai et al. 2005; Kug and Kang 2006; Ohba and Ueda 2007; Yoo et al. 2010; Ohba and Watanabe 2012). The early termination of El Niño has also been attributed to a southward shift of surface wind anomalies during the mature phase associated with the seasonal migration of the western Pacific warm pool (Harrison and Vecchi 1999; Vecchi 2006; McGregor et al. 2012), a feature not distinct during La Niña (Ohba and Ueda 2009; McGregor et al. 2013). The surface wind anomalies are asymmetric between El Niño and La Niña not only in the spatial pattern but also in the amplitude, and larger wind anomalies during El Niño are suggested to result in stronger delayed negative oceanic feedback relative to La Niña (Choi et al. 2013; Dommenges et al. 2013; DiNezio and Deser 2014). With regard to the oceanic nonlinearities, DiNezio and Deser (2014) show that

the delayed thermocline feedback is more effective at terminating El Niño than La Niña because the shoaling thermocline enhances the vertical temperature gradient during the decay phase of El Niño, and the opposite occurs for La Niña, delaying its demise. The shallower thermocline in the western equatorial Pacific is also suggested to result in stronger oceanic wave response to surface wind anomalies during El Niño relative to La Niña (An and Kim 2017, 2018). Besides the dynamical processes, the asymmetry in the thermodynamic air–sea feedback may contribute to the asymmetric evolution of El Niño and La Niña (Chen et al. 2016).

The asymmetry in the duration of El Niño and La Niña is robust for strong events (Okumura and Deser 2010). When we also consider moderate and weak ENSO events, however, the temporal evolution of El Niño and La Niña varies greatly from event to event as shown in the time series of the Niño-3.4 index during 1900–2017 (Fig. 1). Many strong El Niño events terminate quickly after peaking in boreal winter and transition into La Niña events (e.g., 1972–73, 1982–83, and 1997–98), but there are multiple El Niño events that last two years or longer (e.g., 1939–42, 1986–88, and 2014–16). La Niña events following strong El Niño tend to last multiple years. However, this is not always the case (e.g., 1988–89), and there are many long-lasting La Niña events that are not preceded by strong El Niño (e.g., 1954–57, 1970–72, and 2007–09).

The recent frequent occurrence of multiyear La Niña events has drawn attention to the dynamics and predictions of these persistent La Niña events (Hu et al. 2014; DiNezio et al. 2017a,b; Luo et al. 2008, 2017). Hu et al. (2014) show that La Niña tends to return in the second year when the first peak is strong and is not followed by downwelling equatorial Kelvin waves. The generation of downwelling Kelvin waves is associated with surface wind anomalies over the far western equatorial Pacific, although it is not clear what causes these surface wind anomalies. Climate models successfully predict the duration of several observed La Niña events with a 2-yr lead time, and the high predictability is attributed to the oceanic memory related to the preceding El Niño (DiNezio et al. 2017a,b) and the interbasin atmospheric teleconnections (Luo et al. 2017). Despite the multiplicity of studies, the relative importance of oceanic and atmospheric processes on the duration of La Niña has not been assessed in a systematic way. Furthermore, the mechanisms controlling the duration of El Niño events remain largely unknown, beyond a few studies suggesting that the onset timing may affect the duration of El Niño without explicit dynamical explanations (Horii and Hanawa 2004; Lee et al. 2014).

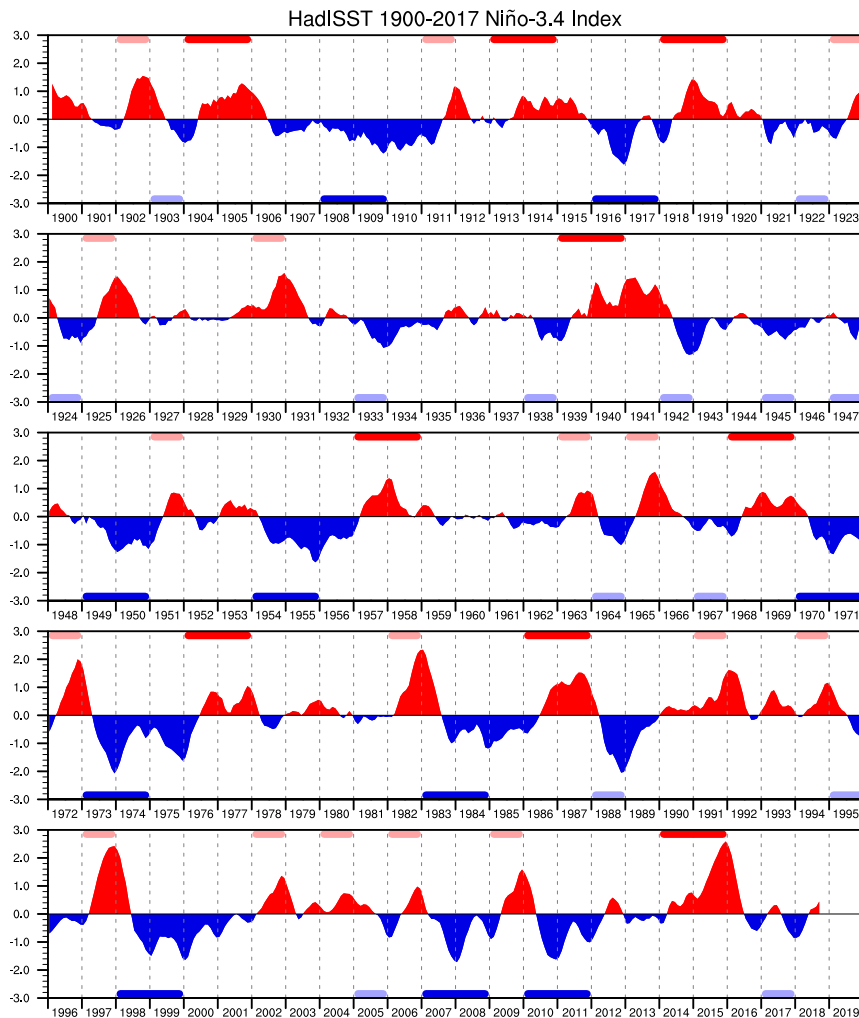


FIG. 1. Time series of the Niño-3.4 index ($^{\circ}\text{C}$) based on the HadISST dataset for 1900–2017. Year 0 of 1-yr (years 0 and 1 of 2-yr) El Niño events are indicated by thick horizontal pink (red) bars along the time axis, and year 0 of 1-yr (years 0 and 1 of 2-yr) La Niña events are given by light-blue (blue) bars. The time series is smoothed with a 3-month running-mean filter.

El Niño and La Niña are known to strongly affect wintertime precipitation over the southern tier of the United States (e.g., Seager and Hoerling 2014; Schubert et al. 2016) and multiyear La Niña events pose a threat of persistent droughts (e.g., Hoerling and Kumar 2003; Hoerling et al. 2013; Okumura et al. 2017b). Therefore, it is crucial to understand the dynamics controlling the duration of El Niño and La Niña to improve the prediction of their persistent climate impacts. In the present study, we investigate the mechanisms causing the variations in the duration of both El Niño and La Niña events through systematic analyses of observational data and a long control simulation of a climate model that reproduces the observed temporal evolution of ENSO events. We address the following questions. What are

the primary factors affecting the duration of El Niño and La Niña events? What are the oceanic and atmospheric processes by which these factors affect the event duration? What other factors external to the ENSO dynamics contribute to the diversity of event duration?

The rest of the paper is organized as follows. The datasets, models, and analysis methods are described in section 2. Section 3 compares the composite evolution of El Niño and La Niña events that last one and two years to identify the primary factors affecting the event duration and examine the underlying oceanic and atmospheric processes. We also explore the factors that cause the diversity of individual event duration. Section 4 summarizes the main results and discusses their implications for future studies.

2. Data and methods

a. Observational datasets

We analyze oceanic and atmospheric processes affecting the duration of El Niño and La Niña events using a suite of observational data. To have a sufficient number of events for the analysis, we choose oceanic and atmospheric datasets that cover the period since 1900. For SST, we use the Hadley Centre Sea Ice and SST dataset (HadISST; Rayner et al. 2003), available for 1870–2017 on a 1° grid. The HadISST data are based on historical in situ ship and buoy observations with satellite data blended in after 1982. The missing grids are filled by optimal interpolation based on empirical orthogonal function analysis. For surface wind components, precipitation, and sea level pressure (SLP), we make use of the Twentieth Century Reanalysis, version 2 (20CR; Compo et al. 2011), available for 1871–2012 on a 2° grid. The 20CR is generated by assimilating only surface pressure and using monthly SSTs and sea ice concentrations from the HadISST data as boundary conditions. For upper-ocean temperature, we make use of the Simple Ocean Data Assimilation reanalysis, version 2.2.4 (SODA; Carton and Giese 2008), available for 1871–2010 on a 0.5° grid with 40 levels in the vertical. The SODA reanalysis is driven by surface winds from the 20CR. Based on this dataset, we estimate the depth of thermocline as the location of the maximum vertical temperature gradient. For all of the datasets, we analyze the period after 1900. Monthly climatologies are calculated for the common data period of 1900–2010 and anomalies from the monthly mean climatology are linearly detrended.

b. CESM1 control simulation

To complement the observational analysis with a limited number of El Niño and La Niña events, we use a 2200-yr preindustrial control simulation of the Community Earth System Model, version 1 (CESM1; Hurrell et al. 2013; Kay et al. 2015). The CESM1 is a state-of-the-art climate model composed of the atmosphere, ocean, land, and cryosphere components linked through a flux coupler. The atmospheric component of CESM1, Community Atmosphere Model, version 5 (CAM5), has upgraded schemes for physical parameterization, including moisture turbulence, shallow convection, cloud macrophysics, and modal aerosol (Neale et al. 2012) relative to its predecessor. The CESM1 control simulation is conducted at nominal 1° latitude–longitude resolution under preindustrial atmospheric greenhouse gas concentrations. We use the model years 400–2200 of the CESM1 control simulation, for which the model exhibits negligible SST trend [$\sim 10^{-7}^\circ\text{C} (100\text{yr})^{-1}$] and small

drift of global ocean temperature [$\sim 0.005^\circ\text{C} (100\text{yr})^{-1}$; Kay et al. 2015]. As for the observational analysis, we compute monthly anomalies by subtracting monthly mean climatology and removing linear trends.

The CESM1 reproduces many key features of tropical Pacific mean climate and variability in observations (DiNezio et al. 2017a). In particular, the simulated ENSO shows a broad spectral peak in the 3–6-yr band, as well as a broad range of amplitude of events, although the overall amplitude of ENSO as measured by standard deviation of SST anomalies in the Niño-3.4 region (5°S – 5°N , 170° – 120°W) is overestimated by $\sim 18\%$ (0.91°C as compared with 0.77°C for the detrended HadISST data during 1900–2017). Importantly, the CESM1 simulates the asymmetry in the pattern and duration of strong El Niño and La Niña events and the diversity in the evolution of individual El Niño and La Niña events as in observations. It is noted that the CESM1 often develops multiyear El Niño events that begin with a year-long weak equatorial warming followed by a rapid growth in the second year (DiNezio et al. 2017a). Similar multiyear El Niño events have been observed (e.g., 2014–16), but these events appear more frequent in the CESM1 control simulation. The analyses of CESM1 are repeated with a 1300-yr preindustrial control simulation of the Community Climate System Model, version 4 (CCSM4; Gent et al. 2011; Deser et al. 2012), a predecessor of CESM1. The results are very similar to those based on CESM1 and therefore are not included in the paper.

c. Definition of 1- and 2-yr El Niño/La Niña events

For both the observational and model analyses, we define El Niño and La Niña events based on SST anomalies averaged in the Niño-3.4 region (5°S – 5°N , 170° – 120°W ; here called the Niño-3.4 index). We denote the year when El Niño and La Niña first develop as year 0 and the months of that year as January⁰, February⁰, . . . , and December⁰. El Niño and La Niña events are respectively defined as occurring when the Niño-3.4 index smoothed with a 3-month running-mean filter is greater than 0.75 standard deviations or less than -0.75 standard deviations in any month from October⁰ to February⁺¹. The standard deviation of the Niño-3.4 index is calculated separately for each calendar month from October to February, ranging from 0.82° to 1°C in observations and from 1° to 1.17°C in CESM1. To understand what distinguishes El Niño and La Niña events that terminate after one year from those lasting two years or longer, we further classify El Niño and La Niña events into 1- and 2-yr events. El Niño and La Niña events are categorized as 2-yr events if the Niño-3.4 index respectively remains above 0.5 standard deviations or below -0.5 standard

deviations in any month during October⁺¹–February⁺² and otherwise are categorized as 1-yr events. The smaller threshold used for the second year reflects that the second peak is weaker than the first peak on average. [Figure 1](#) show time series of the Niño-3.4 index and selections of 1-/2-yr El Niño and La Niña events based on the HadISST data during 1900–2017.

We perform composite and correlation analyses to understand the different evolution of ocean–atmosphere anomalies between 1- and 2-yr events separately for El Niño and La Niña. The statistical significance of the composite and correlation analyses is assessed by means of a Monte Carlo method. For example, the significance of composite mean of X 1-yr El Niño events is tested against a probability density function (PDF) of composite mean based on randomly selected sets of X years. The significance of the composite mean difference between X 1-yr and Y 2-yr El Niño events is tested against a PDF of composite difference based on randomly selected pairs of X and Y years from the pool of 1- and 2-yr El Niño events. The significance of correlation coefficient between two variables is tested against a PDF of correlation coefficient based on randomly reordered variables. For observational (model) analysis, we use 1000 (10000) randomly generated samples to estimate PDFs, and the statistical significance is tested at the confidence level of 80% (98%) based on a two-sided test.

d. CAM5 experiments

The analysis of observational and model data suggests that surface wind anomalies over the western equatorial Pacific play an important role in determining the evolution of El Niño and La Niña events after the mature phase. To test the role of oceanic forcing for these wind anomalies, we conduct a suite of stand-alone CAM5 experiments. For the control experiment, we use a 2600-yr simulation forced with monthly SST climatology from the model years 402–1510 of the CESM1 control simulation, which is conducted as part of the CESM Large Ensemble Project ([Kay et al. 2015](#)). In the first set of experiments, referred to as full tropical experiments, we force CAM5 with monthly SST anomalies composited for 1-/2-yr El Niño and La Niña events from January^{−1} through December⁺² over the tropical oceans (28°S–28°N), with the same climatological SSTs as in the CAM5 control simulation prescribed elsewhere. To avoid discontinuities in SST forcing at the northern and southern boundaries, we apply a linear interpolation between 28° and 35° latitude. Each of these four experiments consists of 20-member ensemble simulations initialized with different atmospheric conditions in which round-off level perturbation unique to each member was made. To test the role of forcing from the different

tropical ocean basins, we conduct two additional sets of experiments by prescribing the composite monthly SST anomalies only over the tropical Indo-Pacific and Pacific (Pacific+Indian and Pacific experiments). All the other experimental protocols follow those for the full tropical experiments. The ensemble-mean atmospheric response in each of the three sets of four experiments is compared with the climatology of the CAM5 control simulation. The statistical significance of the atmospheric responses is assessed through a two-tailed t test at the 90% confidence level.

3. Results

a. Factors affecting the duration of El Niño and La Niña events

To identify the factors affecting the duration of El Niño and La Niña events, we first compare the temporal evolution of the Niño-3.4 index between 1- and 2-yr events ([Fig. 2](#)). Based on the HadISST dataset during 1900–2017, approximately two-thirds of El Niño events terminate after one year (17 events; 65%), while the remaining one-third of El Niño events last two years or longer (9 events; 35%). There are, on the other hand, comparable numbers of La Niña events that terminate after 1 yr and last 2 yr or longer [13 and 10 events (57% and 43%), respectively]. The higher fraction of 2-yr La Niña than 2-yr El Niño is consistent with the overall asymmetry in the duration of El Niño and La Niña reported previously ([Kessler 2002](#); [Larkin and Harrison 2002](#); [McPhaden and Zhang 2009](#); [Ohba and Ueda 2009](#); [Okumura and Deser 2010](#); [Wu et al. 2010](#)). The composite time series of the Niño-3.4 index show that 1-yr El Niño tends to develop a few months earlier and show larger peak amplitude than 2-yr El Niño. The composite Niño-3.4 index also shows a significantly warmer condition during the boreal winter–spring preceding the onset of 1-yr El Niño than that preceding 2-yr El Niño. Consistent with previous studies, the composite analysis shows that 2-yr La Niña tends to be preceded by a stronger warm event in the previous year and to have a larger peak amplitude than 1-yr La Niña. Note that the relation between the peak amplitude and the duration is asymmetric between El Niño and La Niña. 2-yr La Niña also begins to develop slightly later than 1-yr La Niña on average although the difference is not statistically significant. After the mature phase, both 2-yr El Niño and La Niña on average persist through boreal spring despite weakening and start to reintensify in summer, by which 1-yr El Niño and La Niña return to neutral conditions.

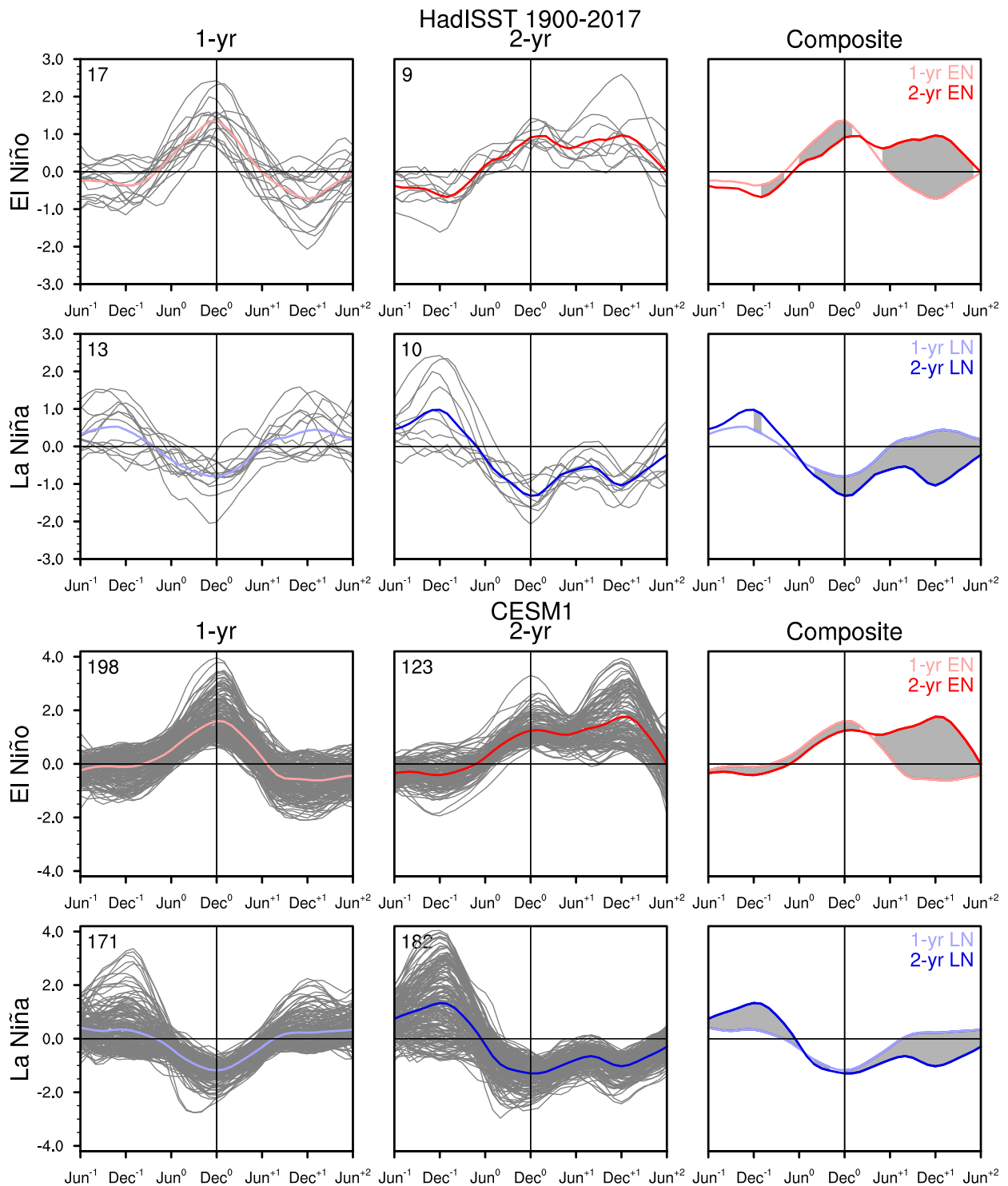


FIG. 2. Time series of the Niño-3.4 index ($^{\circ}\text{C}$) overlaid from Jun^{-1} to Jun^{+2} for (left) 1- and (center) 2-yr (top), (bottom middle) El Niño and (bottom middle), (bottom) La Niña events based on the HadISST during 1900–2017 and the CESM1 control simulation. The time series for individual and composite events are shown by thin gray and thick colored curves, respectively. The number of events is shown at the top-left corner of each panel. Also shown is (right) a comparison of the composite time series in the left and center columns. Gray shading indicates where the difference between the two composites is statistically significant at the 80% or 98% confidence level for the HadISST or CESM1, respectively.

The temporal evolution of observed El Niño and La Niña is well reproduced in the CESM1 control simulation (Fig. 2). The CESM1 simulates the ratios of 1- to 2-yr El Niño and La Niña events comparable to observations (62%:38% and 48%:52%). The composite time series of the Niño-3.4 index also show differences in the amplitude of the preceding events, onset timing, and peak amplitude between 1- and 2-yr events similar to but with greater statistical significance than in observations for both El Niño and La Niña. The CESM1, however, shows a much smaller difference (0.1°C) in the peak amplitude between 1- and 2-yr La Niña events compared to observations (0.5°C). It is also interesting to note that the composite 2-yr El Niño shows larger amplitude in the second than the first year in CESM1 while the peak amplitude is comparable between the first and second years in observations (DiNezio et al. 2017a).

To further evaluate the significance and relative importance of the factors affecting the event duration, we classify observed and simulated El Niño and La Niña events according to the following criteria: the amplitude of the preceding events, onset timing, and peak amplitude. Then we conduct composite analysis of the Niño-3.4 index time series for both El Niño and La Niña events under each criterion (Fig. 3). The preceding event amplitude is defined by the Niño-3.4 index during October⁻¹–February⁰. The event preceding La Niña is categorized as a strong event when the Niño-3.4 index is greater than 1.5 standard deviations in any month during October⁻¹–February⁰, and otherwise as a weak event. For El Niño, we use the threshold value of -0.5 standard deviations. These asymmetric threshold values for El Niño and La Niña reflect the fact that nearly one-half of La Niña events are preceded by El Niño whereas very few El Niño events develop from La Niña. (Preceding “events” are not necessarily ENSO events.) The onset timing is defined as the month when the absolute value of the Niño-3.4 index first exceeds 0.5°C in observations and 0.65°C in CESM1 for both El Niño and La Niña. The larger threshold value for the CESM1 reflects the larger ENSO amplitude relative to observations. The onset in/before and after June is classified as early and late onset, respectively, based on the distribution of onset months for all events (cf. Fig. 9, below). The peak amplitude of El Niño and La Niña is defined by the Niño-3.4 index during October⁰–February⁺¹. El Niño and La Niña are categorized as a strong event when the absolute value of the Niño-3.4 index is greater than 1.5 standard deviations in any month during October⁰–February⁺¹, and otherwise as a weak event.

The composite analysis based on the three criteria indicates that the onset timing has the largest impact on the duration of El Niño events in both observations and

CESM1 (Fig. 3). For El Niño, the three factors are not independent of each other, and an event that develops earlier tends to be preceded by a warmer condition in the previous year and to develop into a stronger event. For La Niña, on the other hand, the observations and CESM1 agree that both the preceding event amplitude and the peak amplitude significantly affect the event duration. The peak amplitude of La Niña is, in turn, linked to the amplitude of the preceding warm events, which affects the magnitude of initial discharge of the equatorial oceanic heat content (DiNezio et al. 2017a). Strong preceding warm events, however, do not necessarily lead to strong La Niña in CESM1, presumably because they also delay the onset of La Niña and shorten the growth time before the mature phase.

The existence of early precursors, namely, the onset timing for El Niño and the amplitude of the preceding events for La Niña, suggests potential predictability of the event duration and requires further understanding of the mechanisms underlying their linkages. The rest of this section explores the oceanic and atmospheric processes by which the three factors affect the duration of El Niño and La Niña events by comparing the composite evolution of 1- and 2-yr events. Because of the overall similarity between the observations and models, we mainly present the results based on the CESM1 control simulation but discuss any discrepancies in observations.

b. Role of oceanic adjustments

The long lead time of the precursors for the duration of El Niño and La Niña events is indicative of the role of slow oceanic adjustments. It is known that SST anomalies associated with El Niño and La Niña are preceded by vertical displacement of the thermocline and associated changes in the equatorial oceanic heat content. Thus, we compare the composite evolution of thermocline depth anomalies in CESM1 between 1- and 2-yr events along a path from the northern tropical Pacific (6°–12°N) to the equatorial Pacific (3°S–3°N), together with SST and surface wind anomalies (Fig. 4; see Fig. S2 in the online supplemental material for the statistical significance of these composites). Note that the ENSO cycle in CESM1 is strongly influenced by off-equatorial Rossby waves forced by wind stress curl anomalies, which maximize in the latitude band of 6°–12°, while equatorial Rossby wave (maximize in latitude band 5°–7°) appear to play a more important role in observations (Fig. S1 of the online supplemental material). For both 1- and 2-yr events, El Niño and La Niña are preceded by basinwide deepening and shoaling of the equatorial thermocline, respectively, in support of the recharge oscillator mechanism (Jin 1997; Meinen and McPhaden 2000). The magnitude of initial

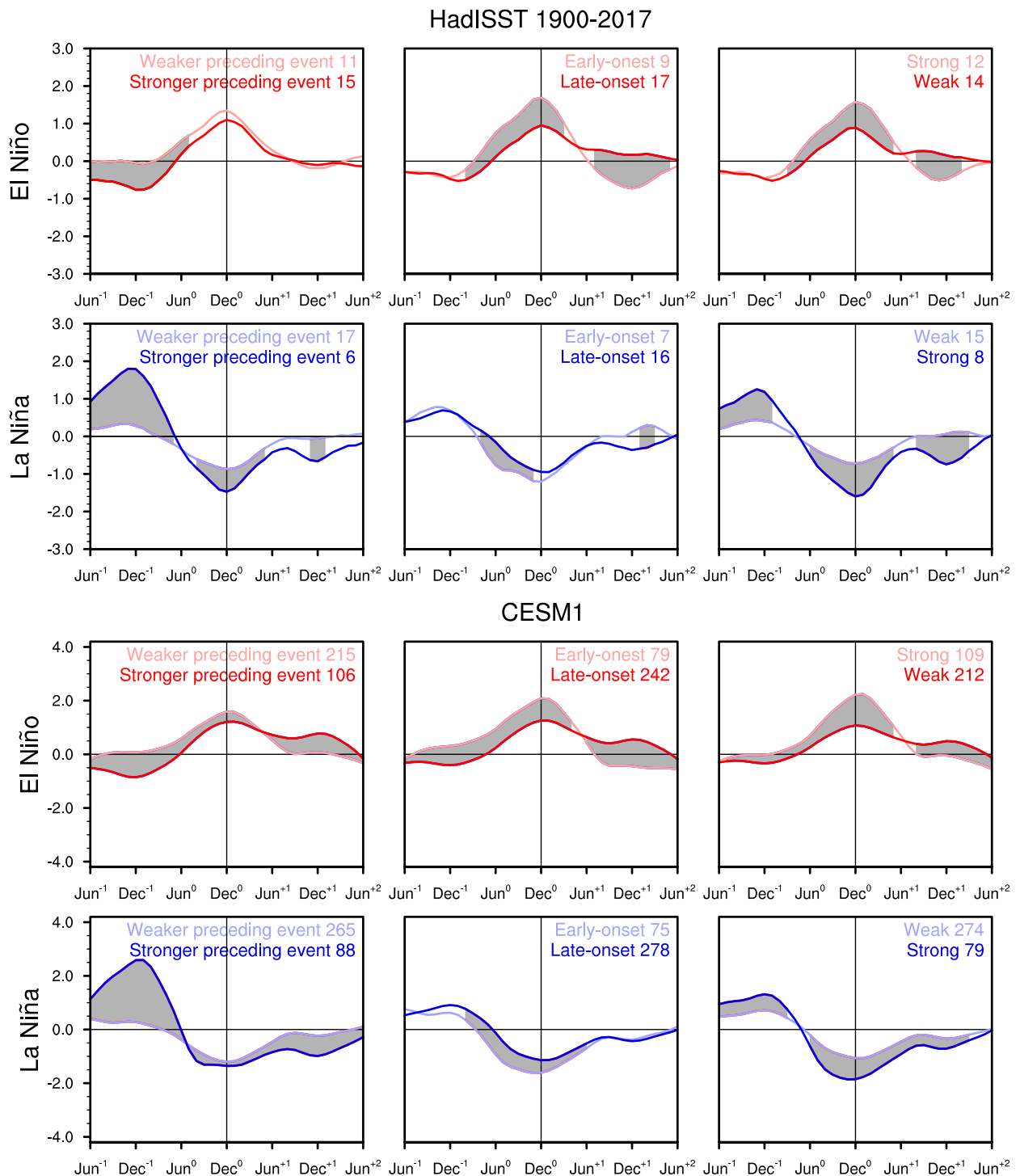


FIG. 3. Time series of the Niño-3.4 index ($^{\circ}\text{C}$) from June⁻¹ to June⁺² for (top),(bottom middle) El Niño and (bottom middle),(bottom) La Niña events composited according to (left) the amplitude of the preceding event, (center) onset timing, and (right) peak amplitude based on the HadISST during 1900–2017 and the CESM1 control simulation. The number of events used for the composites is shown at the top-right corner of each panel. Gray shading indicates where the difference between the two composites is statistically significant at the 80% or 98% confidence level for the HadISST or CESM1, respectively. See the text for the criteria used to classify El Niño and La Niña events.

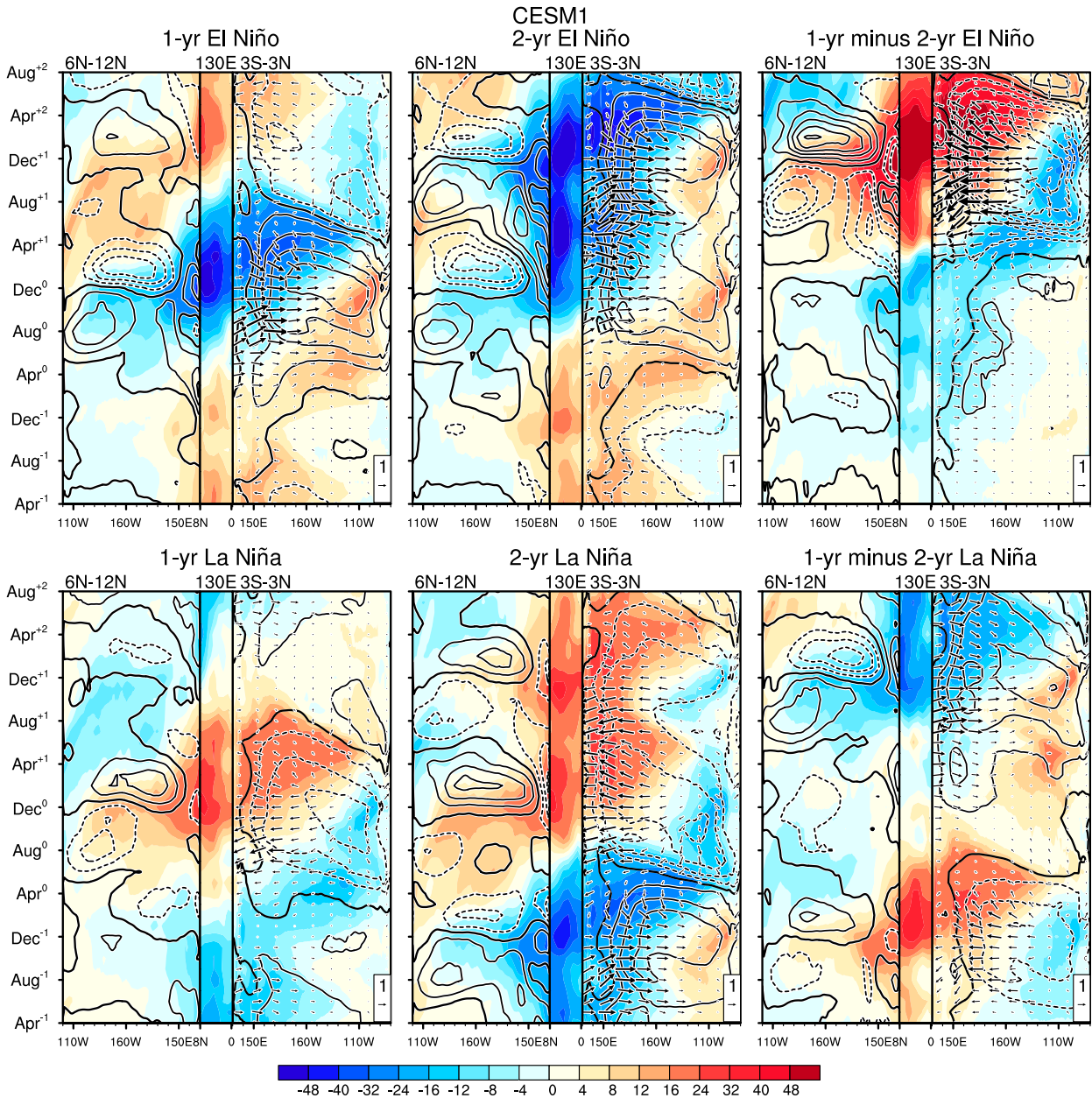


FIG. 4. Longitude–time sections of composite thermocline depth anomalies (m; shading) along the off-equatorial (6° – 12° N), western Pacific boundary (130° E), and equatorial (3° S– 3° N) waveguides from April $^{-1}$ to August $^{+2}$ for (left) 1- and (middle) 2-yr (top) El Niño and (bottom) La Niña events based on the CESM1 control simulation. Also shown is (right) the difference between the left and center columns. In the equatorial segment, SST ($^{\circ}$ C; contours at intervals of 0.4; zero contours thickened) and surface wind (m s^{-1} ; vectors) anomalies are overlaid. In the off-equatorial segment, wind stress curl anomalies (N m^{-3} ; contours at intervals of 10^{-8} ; zero contours thickened) are overlaid. Note that the longitude axis is reversed for the off-equatorial segment to better show the Rossby wave reflection at the western boundary. The statistical significance of these anomalies is shown in supplemental Fig. S2.

thermocline depth anomalies is larger for 2-yr than 1-yr events for both El Niño and La Niña, presumably because of the larger amplitude of preceding event for 2-yr events. Reflecting the stronger tendency for La Niña to be preceded by the opposite phase of ENSO than for El Niño, the magnitude of discharge prior to La Niña is larger

than the magnitude of recharge prior to El Niño. After the onset of El Niño and La Niña, surface zonal wind anomalies over the western-central equatorial Pacific force an oceanic equatorial Kelvin wave, inducing thermocline depth anomalies in the eastern equatorial Pacific during the equatorial cold season. At the same time, an

off-equatorial Rossby wave forced by wind stress curl anomalies travels westward, which upon reaching at the western boundary propagates equatorward as a coastal Kelvin wave and then reflects as an equatorial Kelvin wave around the mature phase, in accordance with the delayed oscillator mechanism (e.g., Suarez and Schopf 1988; Battisti and Hirst 1989; Schneider et al. 1995; Kirtman 1997). During 1-yr El Niño and La Niña, this Rossby wave reflection results in a reversal of thermocline depth anomalies in the eastern equatorial Pacific by April⁺¹. During 2-yr El Niño and La Niña, on the other hand, the thermocline depth anomalies in the eastern equatorial Pacific remain of the same sign throughout year +1. The sign of thermocline depth anomalies in the eastern equatorial Pacific, rather than those averaged across the equatorial Pacific, appears to be a good indicator of the evolution of both El Niño and La Niña in the second year.

What causes the distinct thermocline depth anomalies in the eastern equatorial Pacific between 1- and 2-yr events? For El Niño, the large difference in thermocline depth anomalies in April⁺¹ is clearly associated with the reflection of upwelling Rossby wave (Fig. 4, top right). While the upwelling Rossby wave has comparable magnitude between 1- and 2-yr El Niño at the western boundary, the generation and reflection of Rossby wave occur a few months earlier during 1-yr El Niño than during 2-yr El Niño because of the earlier onset of 1-yr El Niño. During 2-yr El Niño, the upwelling Kelvin wave reflected from the western boundary does not arrive at the eastern equatorial Pacific by the end of boreal spring, and El Niño starts to reintensify in the following summer, when the seasonal development of the equatorial cold tongue strengthens the Bjerknes feedback (e.g., Mitchell and Wallace 1992; Stein et al. 2014). Thus, the onset timing appears to control the duration of El Niño events by affecting the timing of delayed oceanic feedback.

In contrast, the different evolution of thermocline depth anomalies between 1- and 2-yr La Niña is strongly associated with the magnitude of initial heat content discharge (Fig. 4, bottom right), in agreement with previous studies (DiNezio and Deser 2014; DiNezio et al. 2017a,b). There is no significant difference in the timing and amplitude of reflected Rossby wave between 1- and 2-yr La Niña. During 2-yr La Niña, the large initial discharge of the equatorial oceanic heat content prevents the reversal of thermocline depth anomalies in the eastern equatorial Pacific against the downwelling Kelvin wave reflected from the western boundary. Thus, the oceanic memory of previous warm event appears to play an important role in determining the duration of La Niña.

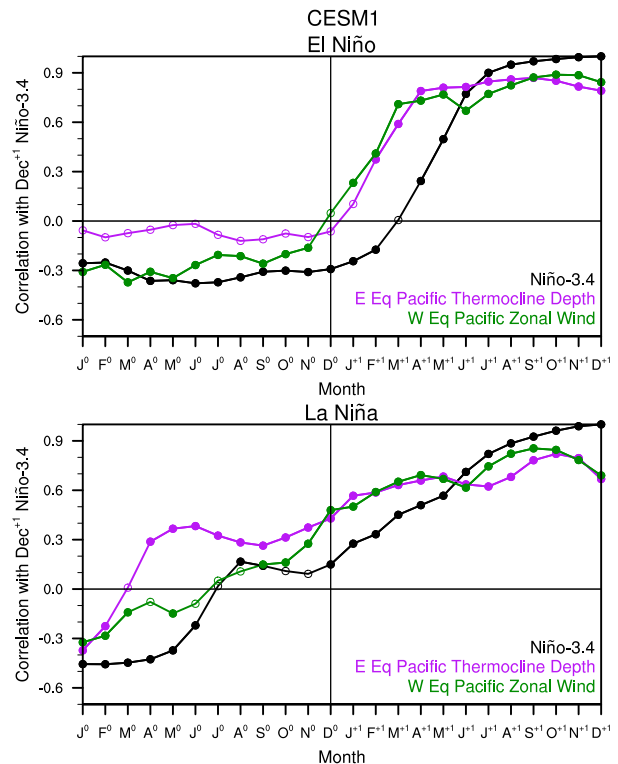


FIG. 5. Correlations of the December⁺¹ Niño-3.4 index with the Niño-3.4 index (black), thermocline depth anomalies in the eastern equatorial Pacific (3°S–3°N, 150°–80°W; purple), and zonal wind anomalies over the western equatorial Pacific (3°S–3°N, 130°–170°E; green) during January⁰–December⁺¹ of (top) El Niño and (bottom) La Niña events in the CESM1 control simulation. The filled circles indicate correlations that are statistically significant at the 98% confidence level.

To corroborate the role of oceanic adjustment in affecting the event duration, we conduct correlation analysis of the December⁺¹ Niño-3.4 index with the thermocline depth anomalies in the eastern equatorial Pacific (3°S–3°N, 150°–80°W) during years 0 and +1 of El Niño and La Niña in CESM1 (Fig. 5, purple curves). Here the December⁺¹ Niño-3.4 index is used as a proxy of the event duration (larger positive and negative values indicate longer duration of El Niño and La Niña, respectively). In agreement with the composite analysis (Fig. 4), the thermocline depth anomalies in the eastern equatorial Pacific become highly correlated ($r > 0.6$) with the December⁺¹ Niño-3.4 index after April⁺¹ for both El Niño and La Niña, leading the development of Niño-3.4 SST anomalies by a few months (Fig. 5, black curves). For El Niño, these thermocline depth anomalies affecting the event duration develop very rapidly from January⁺¹ to April⁺¹, coincidentally with the timing of the upwelling Rossby wave reflection. For La Niña, on the other hand, the thermocline depth anomalies affecting

the event duration can be traced back to boreal spring of year 0, indicating the influence of the heat content discharge associated with the previous warm event. The observations agree on the role of delayed feedback for El Niño and oceanic memory for La Niña in the thermocline adjustment although the observational analysis suffers from the lack of samples (supplemental Fig. S3).

Besides the oceanic adjustment processes, the distinct temporal evolution of thermocline depth anomalies between 1- and 2-yr events is associated with the different evolution of surface wind anomalies along the equator for both El Niño and La Niña (Figs. 4 and S1). During 1-yr El Niño and La Niña events, zonal wind anomalies decay rapidly over the western equatorial Pacific from the mature phase to the following boreal spring, while they change little during 2-yr events. The weakening of zonal wind anomalies would aid the termination of events by enhancing the delayed negative oceanic feedback. The rapid decay of surface wind anomalies begins during the mature phase of 1-yr events and therefore cannot be explained by changes in equatorial Pacific SST anomalies. Conversely, these changes in surface wind anomalies lead the changes in Niño-3.4 SST anomalies by a few months (Figs. 5 and S3, green curves). This result is indicative of the role of atmospheric adjustment in affecting the duration of El Niño and La Niña events, which is explored further in the next section.

c. Role of atmospheric adjustment

What causes the rapid decay of surface wind anomalies over the western equatorial Pacific after the mature phase of 1-yr El Niño and La Niña? To explore the origin of these surface wind changes in CESM1, we compare the composite maps of tropical surface winds, SST, and precipitation anomalies between 1- and 2-yr events for February⁺¹–March⁺¹ (Fig. 6, top three rows; see supplemental Fig. S5 for the statistical significance), when the significant difference in surface wind anomalies develops over the western equatorial Pacific (Figs. 4 and 5). For both El Niño and La Niña, the difference in surface wind anomalies is not limited to the western equatorial Pacific but extends over the Indian Ocean and the tropical North Pacific. The development of easterly wind anomalies during 1-yr El Niño relative to 2-yr El Niño is associated with overall cooling of the tropical Pacific, particularly the region extending from the western equatorial Pacific to the northeastern tropical Pacific, and warming of the Indian and Atlantic Oceans. Similarly, the development of westerly wind anomalies during 1-yr La Niña relative to 2-yr La Niña is associated with overall warming of the tropical Pacific and cooling of the Indian and Atlantic Oceans. In

relation to these changes in the interbasin SST gradient, precipitation tends to increase over the warmer oceans and decrease over the cooler oceans, which would drive the changes in equatorial zonal winds through adjustments of the Walker circulation. The difference between 1- and 2-yr El Niño also shows a zonal dipole pattern of SST and precipitation anomalies in the equatorial Pacific, indicating an eastward shift of equatorial ocean–atmosphere anomalies during 1-yr El Niño relative to 2-yr El Niño. This result is not inconsistent with previous studies that attribute the shorter duration of El Niño relative to La Niña to the more eastward location of ocean–atmosphere anomalies in the equatorial Pacific, which makes the western Pacific more susceptible to negative feedback from the Indian Ocean (Okumura and Deser 2010; Okumura et al. 2011). The difference between 1- and 2-yr La Niña, on the other hand, indicates that the equatorial Pacific cooling is much stronger for 2-yr than 1-yr event in the far western equatorial Pacific, which is not captured well in the composite time series of the Niño-3.4 index (Fig. 2). These results of CESM1 generally agree with the analysis of observations, although the Indian Ocean shows stronger cooling for 2-yr than 1-yr La Niña in observations contrary to the model (supplemental Fig. S4).

To test the role of oceanic forcing for the different evolution of surface wind anomalies between 1- and 2-yr events, we analyze a suite of CAM5 experiments forced with tropical SST anomalies composited for El Niño and La Niña events in CESM1 (Fig. 6, bottom three rows; see Fig. S5 for the statistical significance). In response to the full tropical SST forcing, CAM5 indeed reproduces the difference in surface wind and precipitation anomalies over the equatorial Pacific in February⁺¹–March⁺¹ for both El Niño and La Niña, albeit with smaller amplitude for El Niño relative to the CESM1 composite. A comparison with additional sets of experiments in which tropical SST anomalies outside the Pacific are removed indicates that the Indian Ocean warming plays a critical role in driving easterly wind anomalies over the western equatorial Pacific for El Niño. For La Niña, on the other hand, the Pacific warming alone forces large part of westerly wind anomalies over the western equatorial Pacific, while the Atlantic cooling plays a more important role in the central equatorial Pacific. These impacts of Indian and Atlantic Ocean SSTs on Pacific surface winds are consistent with previous observational and modeling studies (Annamalai et al. 2005; Kug and Kang 2006; Ohba and Ueda 2007; Yoo et al. 2010; Izumo et al. 2010; Okumura et al. 2011; Wang 2006; Rodríguez-Fonseca et al. 2009; Jansen et al. 2009; Ding et al. 2012; Keenlyside et al. 2013; Ham and Kug 2015; Polo et al. 2015; McGregor et al. 2014; Li et al. 2016; Wang et al.

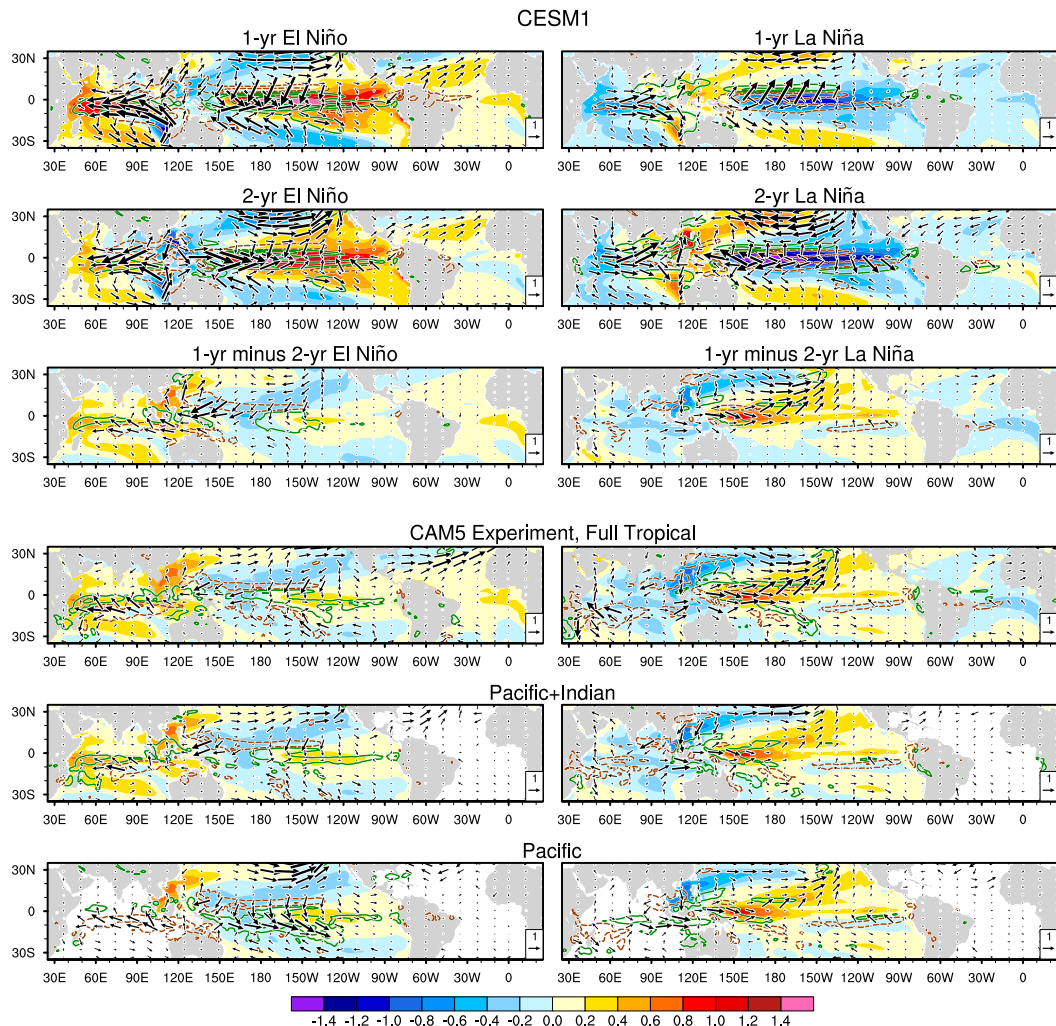


FIG. 6. Composite maps of February⁺¹–March⁺¹ SST ($^{\circ}\text{C}$; shading), surface wind (m s^{-1} ; vectors), and precipitation [positive (negative) contours in green solid (brown dashed) at $\pm 1, 3, 5, \dots$ mm day^{-1}] anomalies for (top) 1- and (second row) 2-yr (left) El Niño and (right) La Niña events based on the CESM1 control simulation, along with (third row) the difference between the top and second rows. The bottom half of the figure is similar to the third row but is based on the ensemble-mean response in the (fourth row) full tropical, (fifth row) Pacific+Indian, and (bottom) Pacific CAM5 experiments. The statistical significance of these anomalies is shown in supplemental Fig. S5.

2017; Cai et al. 2019). The muted easterly wind response over the western equatorial Pacific in the CAM5 El Niño experiments also suggests a role of atmospheric processes unrelated to the tropical SST forcing or small-scale SST variations unresolved in the composite SST forcing. In particular, we note that these easterly wind anomalies are part of an anticyclonic circulation anomaly over the tropical North Pacific in CESM1, which is not reproduced in any of the CAM5 experiments. This disagreement suggests that stochastic atmospheric variability in the North Pacific, such as the North Pacific Oscillation (NPO), may play a role in affecting surface wind anomalies and the duration of El Niño events.

What causes the difference in interbasin SST gradient anomalies between 1- and 2-yr events after the mature phase of El Niño and La Niña in the first place? To address this question, Fig. 7 compares the temporal evolutions of SST and surface wind anomalies in CESM1 between 1- and 2-yr events along the entire equator (see supplemental Fig. S7 for the statistical significance). The equatorial Pacific warming associated with El Niño induces delayed warming of the Atlantic and Indian Oceans starting around the mature phase through adjustments of the Walker circulation [see Xie and Carton (2004), Chang et al. (2006), and Schott et al. (2009) for reviews]. Similarly, the equatorial Pacific

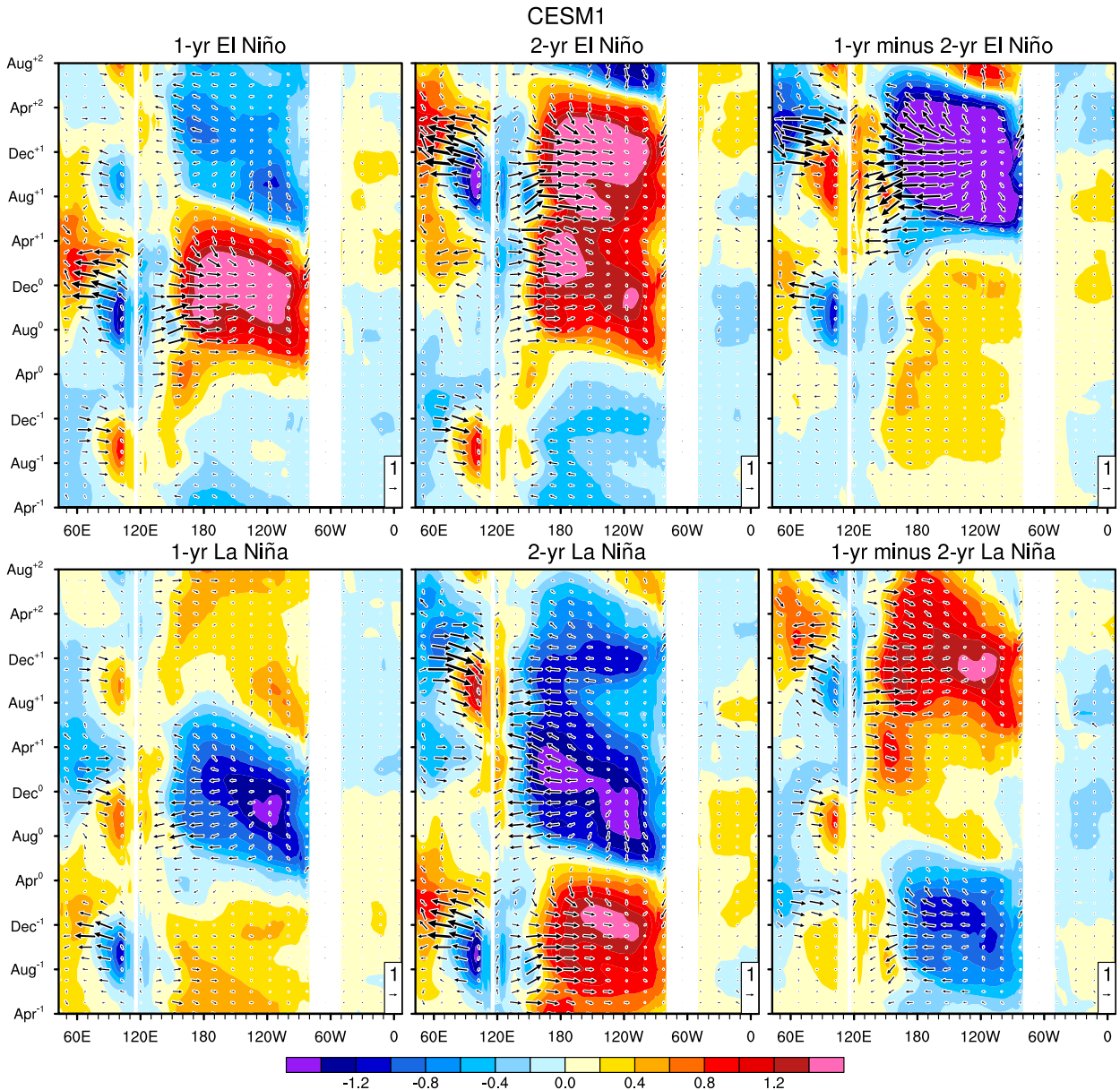


FIG. 7. Longitude–time sections of composite SST ($^{\circ}\text{C}$; shading) and surface wind (m s^{-1} ; vectors) anomalies along the equator (3°S – 3°N ; 10°S – 0° in the Indian Ocean) from April^{−1} to August⁺² for (left) 1- and (center) 2-yr (top) El Niño and (bottom) La Niña events based on the CESM1 control simulation. Also shown is (right) the difference between the left and center columns. The statistical significance of these anomalies is shown in supplemental Fig. S7.

cooling associated with La Niña induces delayed cooling of the Atlantic and Indian Oceans. The earlier onset and larger amplitude of 1-yr El Niño relative to 2-yr El Niño lead to an earlier and larger warming of the Atlantic and Indian Oceans. As a result, positive anomalies of the interbasin SST gradient, defined as an SST difference between the Pacific and Atlantic/Indian Oceans, start to decrease one month before the mature phase during 1-yr El Niño (Fig. 8). Concurrently, surface westerly wind

anomalies weaken over the western equatorial Pacific, followed by a rapid shoaling of the thermocline in the eastern equatorial Pacific. For La Niña, the different evolution of interbasin SST gradient anomalies between 1- and 2-yr events is linked more to the amplitude of previous warm event in the Pacific (Figs. 7 and 8). The strong equatorial Pacific warming preceding 2-yr La Niña induces not only strong Pacific cooling but also strong delayed warming of the Indian and Atlantic

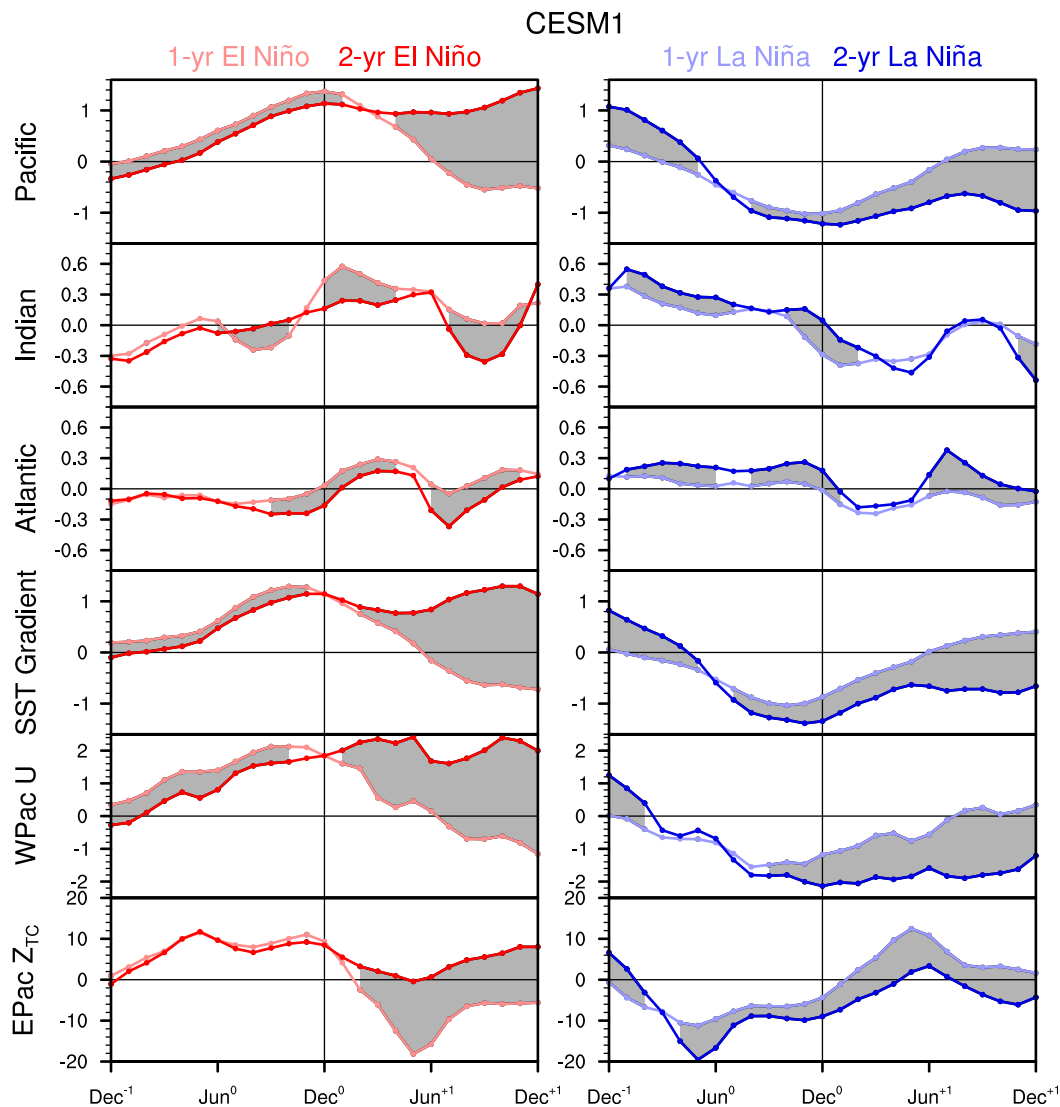


FIG. 8. Time series of composite equatorial anomalies (3°S – 3°N) of SST ($^{\circ}\text{C}$) in the Pacific (140°E – 80°W), Indian (40°E – 100°E), and Atlantic (50°W – 15°E) Oceans, interbasin SST gradient between the Pacific and Indian/Atlantic Oceans (140°E – 80°W minus 50°W – 100°E ; $^{\circ}\text{C}$), and thermocline depth in the eastern Pacific (150° – 80°W ; m) from December⁻¹ to December⁺¹ for 1- and 2-yr (left) El Niño and (right) La Niña events based on the CESM1 control simulation. The curves with dark colors show composites for 2-yr events. Gray shading indicates where the difference between the two composites is statistically significant at the 98% confidence level.

Oceans, which together help maintain the negative SST gradient anomalies toward the Pacific through the boreal spring following the mature phase. The lack of this effect during 1-yr La Niña results in the earlier decay of negative interbasin SST gradient anomalies, which may contribute to the rapid reduction in surface wind and thermocline depth anomalies. The observations show similar difference in the evolution of interbasin SST gradient anomalies between 1- and 2-yr events for both El Niño and La Niña, although the difference in Atlantic

and Indian Ocean SST anomalies between 1- and 2-yr La Niña is not very significant in observations (supplemental Figs. S6 and S8). We also note that the timing of the decay of surface wind anomalies over the western equatorial Pacific differs in observations. In particular, surface wind anomalies start to decrease with the warming of the Indian and Atlantic Oceans during observed 1-yr El Niño.

The comparison of SST anomaly evolution in Fig. 7 also reveals that Indian Ocean dipole (IOD), which

often develops in boreal summer–fall preceding the mature phase of El Niño and La Niña, is stronger during 1-yr than 2-yr events for both El Niño and La Niña, as noted by Okumura et al. (2017a). During 1-yr El Niño, the strong positive IOD may enhance the subsequent basinwide warming of the Indian Ocean (Hong et al. 2010) and hasten the event termination. The different strength of IOD between 1- and 2-yr events is likely related to the different timing of their onset as suggested by Nagura and Konda (2007), but it may also indicate the active role of IOD independent of ENSO in modulating the duration of El Niño and La Niña events, which is explored further in the next section. The difference in IOD between 1- and 2-yr events is similar in observations and CCSM4, except the strength of IOD is comparable between 1- and 2-yr La Niña in observations (Fig. S6).

d. Factors external to the ENSO dynamics

The composite analysis of the Niño-3.4 index stratified by the onset month for El Niño and the amplitude of preceding events for La Niña reaffirms the importance of these factors in determining the event duration in both observations and CESM1 (Fig. 9, line plots). These factors are nearly linearly related to the event duration in the composite analysis, with the duration of El Niño and La Niña events becoming progressively longer with later onset months and larger amplitude of preceding warm events, respectively (Fig. 9, scatterplots). However, individual events deviate greatly from the linear relationship. In CESM1, El Niño events that have onset after June show a large spread in their duration regardless of the overall tendency to last 2 years, whereas those that develop before or in June mostly terminate after 1 year. Similarly, La Niña events not following a strong warm event (December⁻¹ Niño-3.4 < 1.5°C) show diverse duration, although those following a strong warm event usually continue into the second year. Observations show similar results, although it is difficult to assess the spread of individual event duration because of the small sample size. It is noted that in observations all El Niño events have onset after May (13% El Niño onset before May in CESM1) and those that have onset after September show more tendency to last 2 years.

To identify the factors affecting the duration of individual events in CESM1, we correlate the December⁺¹ Niño-3.4 index with SST and surface wind anomalies along the equator from April⁻¹ to August⁺² of El Niño and La Niña events in CESM1 (Fig. 10, top; see supplemental Fig. S9 for the statistical significance). The December⁺¹ Niño-3.4 index shows significant negative correlations with equatorial Pacific SST anomalies in

boreal spring–summer of year 0 for El Niño and fall of year -1 through spring of year 0 for La Niña, confirming the importance of the onset timing and preceding event amplitude to the duration of El Niño and La Niña, respectively. For both El Niño and La Niña, the SST correlations become significant in the equatorial Atlantic and Indian Oceans in summer–fall of year 0. The Indian Ocean SST correlations show a negative IOD pattern in summer–fall and transition into a basinwide cooling pattern after the mature phase, while the Atlantic SST correlations show a basinwide cooling pattern from fall through winter. The December⁺¹ Niño-3.4 index is also significantly correlated with surface winds over the western equatorial Pacific in spring following the mature phase, when the negative SST correlations develop across the Atlantic and Indian Oceans. These results confirm the importance of interbasin SST adjustments and resultant changes in surface winds for the duration of El Niño and La Niña.

To further isolate the factors affecting the event duration unrelated to the onset timing for El Niño and the preceding event amplitude for La Niña, we conduct the same correlation analysis with the December⁺¹ Niño-3.4 index after removing the linear regressions on these factors from the SST and surface wind fields (Fig. 10, bottom). The resultant SST correlations remain strikingly similar outside the equatorial Pacific after summer–fall of year 0. This result indicates that variability of the Atlantic and Indian Oceans unrelated to the ENSO strongly affects the duration of ENSO events by modulating the interbasin SST gradient. It is not very clear why a negative IOD leads to a basinwide cooling after the mature phase, which requires further investigation. It is worth noting that SST correlations show a weak zonal dipole pattern in the equatorial Pacific for El Niño, suggesting that the pattern of Pacific warming affects the El Niño duration (e.g., a warming shifted more to the west tends to last longer). The pattern of warming may also influence variability over the Atlantic and Indian Oceans.

To explore the role of ocean–atmosphere variability outside the equatorial region in affecting the duration of El Niño and La Niña events in CESM1, we expand the lead–lag correlation analysis based on the December⁺¹ Niño-3.4 index into the global domain. An examination of monthly correlation maps indicates that the recurrence of both El Niño and La Niña events in the second year is associated with a meridional dipole pattern of SLP anomalies over the North Pacific that resembles the NPO during January⁺¹–March⁺¹ (Fig. 11). The NPO is known to arise from internal atmospheric dynamics and has been suggested to trigger some ENSO events by imposing a seasonal “footprint” on

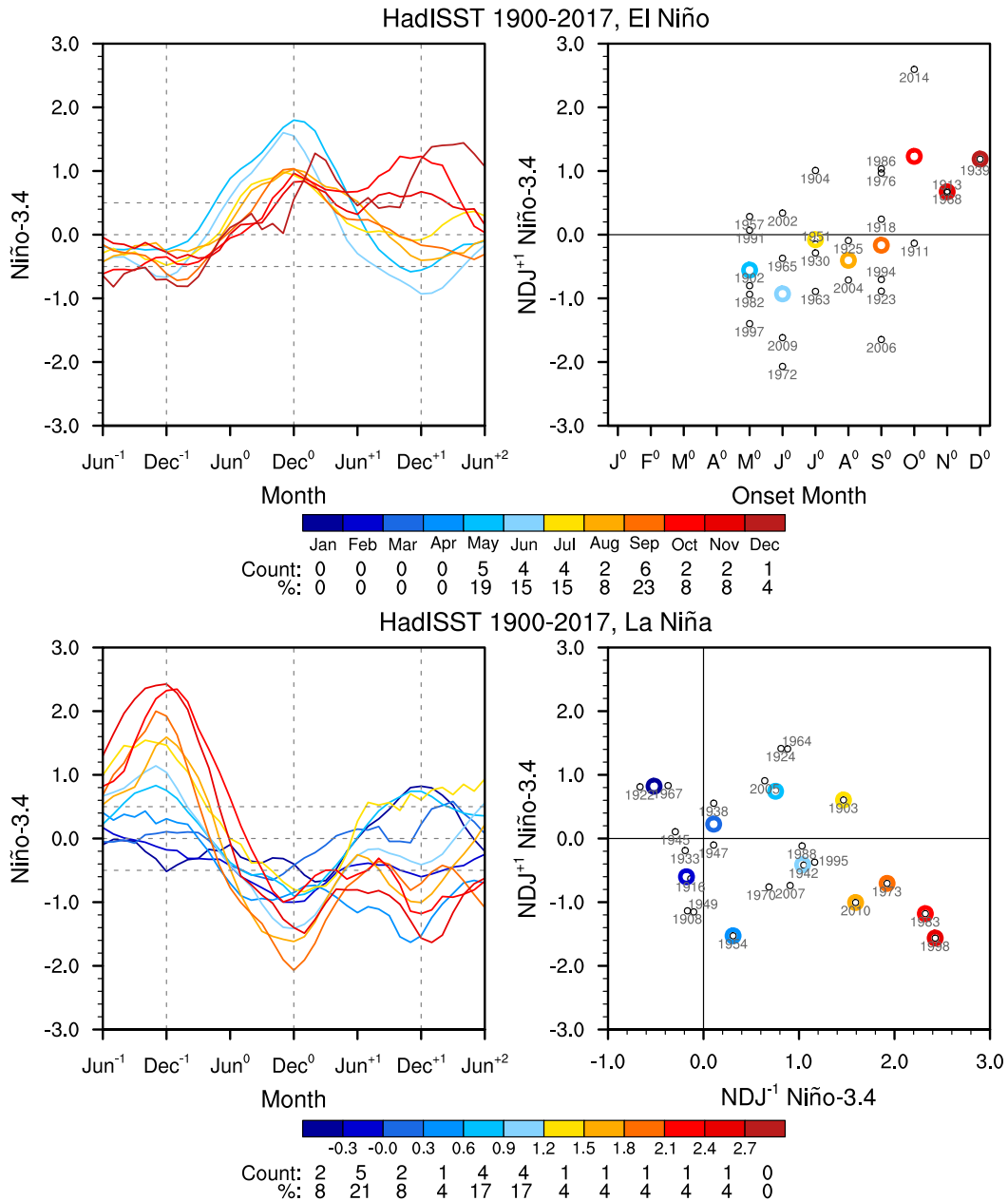


FIG. 9. Time series (the line plots) of the Niño-3.4 index (°C) composited for (top) El Niño events categorized by onset month and (bottom) La Niña events categorized by the magnitude of the December⁻¹ Niño-3.4 index based on the HadISST dataset and CESM1 control simulation. The colors of composite curves correspond to the categorization criteria shown on color bars. The number under the color bars indicates the count and percentage of events used in each composite. Also shown are scatterplots of the November–January⁺¹ (for HadISST) or December⁺¹ (for CESM1) Niño-3.4 index vs (top) the onset month for El Niño events and (bottom) the November–January⁻¹ (for HadISST) or December⁻¹ (for CESM1) Niño-3.4 index for La Niña events. Small open black circles indicate individual events, and large colored circles represent composite events. Note that the Niño-3.4 index is smoothed with a 3-month running-mean filter prior to the analysis of the HadISST dataset.

subtropical SSTs during boreal winter–spring (e.g., Vimont et al. 2001, 2003; Anderson 2003; Chang et al. 2007; Alexander et al. 2010). It is plausible that the NPO during and after the mature phase of ENSO

affects the evolution of events in the second year and hence the duration. However, it is unclear to what degree the NPO pattern of SLP correlations is independent of tropical SST forcing during January⁺¹–March⁺¹,

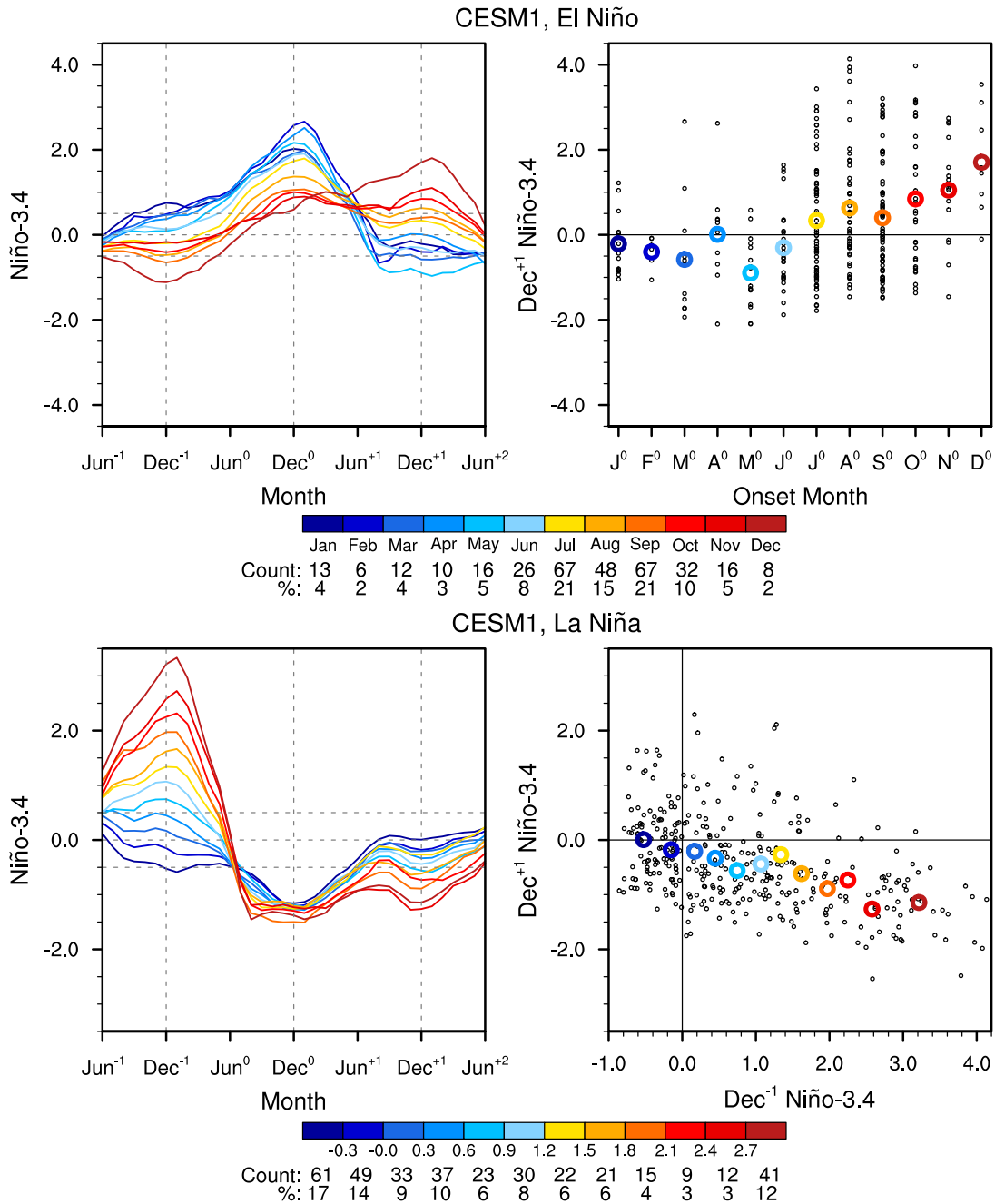


FIG. 9. (Continued).

when El Niño and La Niña already show the sign of recurrence. The composite analysis based on CESM1 shows similar patterns of SLP and tropical SST anomaly differences between 1- and 2-yr events (Fig. 12, third row). Interestingly, the CAM5 experiments forced with these tropical SST anomalies reproduce the meridional dipole pattern of SLP anomalies albeit with weaker amplitude (Fig. 12, bottom row). Therefore, the NPO pattern of SLP anomalies

associated with the event duration is likely to arise from both tropical SST forcing and internal atmospheric variability. The CAM5 experiments with partial tropical SST forcing suggest that zonally asymmetric patterns of SST anomalies over the tropical Pacific are most important in forcing the NPO pattern of SLP anomalies (not shown).

Figure 13 examines the influences of IOD in September⁰–November⁰, equatorial Atlantic SST variability in November⁰–January⁺¹, and the NPO in

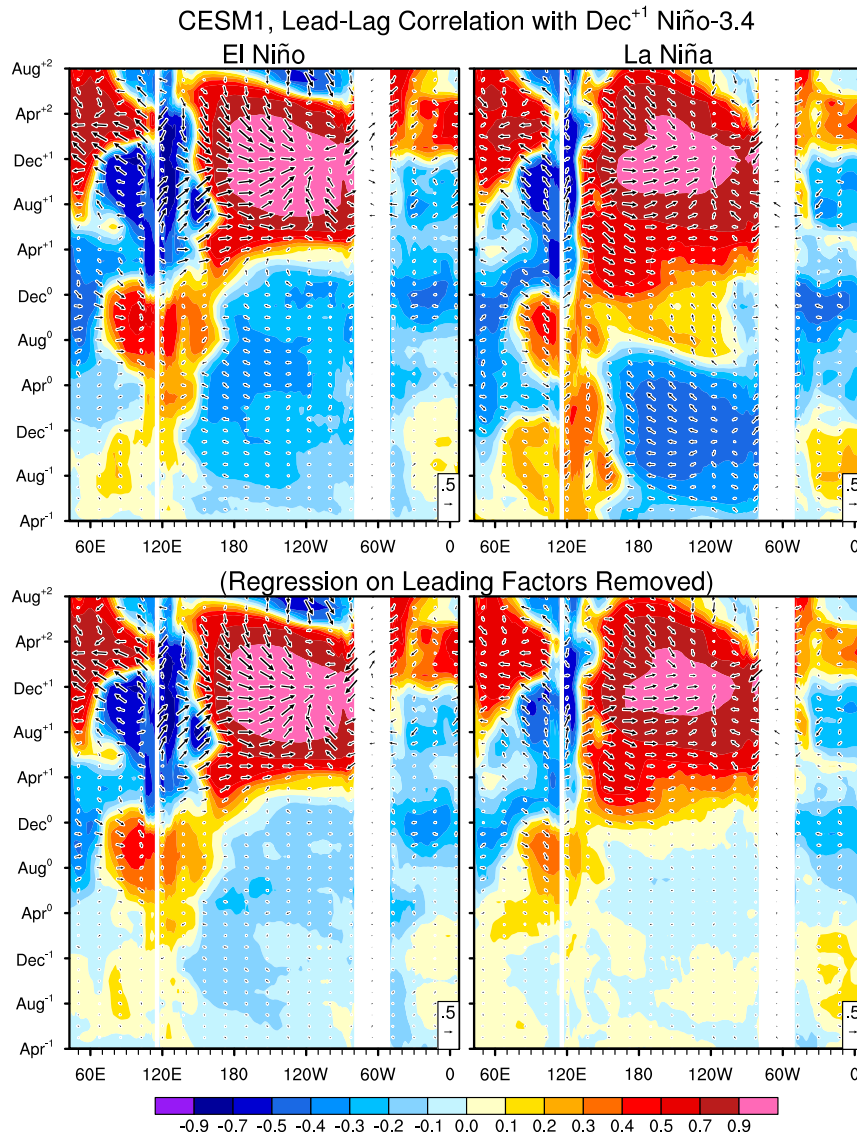


FIG. 10. (top) Lead-lag correlations of the December⁺¹ Niño-3.4 index with SST (°C; shading) and surface wind (m s^{-1} ; vectors) anomalies along the equator (3°S – 3°N ; 10°S – 0° in the Indian Ocean) from April⁻¹ to August⁺² for (left) El Niño and (right) La Niña events based on the CESM1 control simulation. (bottom) As in the top panels, but linear regressions on the onset month for El Niño and the December⁻¹ Niño-3.4 index for La Niña are removed from the December⁺¹ Niño-3.4 index and equatorial SST and surface wind anomalies prior to the correlation analysis. The statistical significance of these anomalies is shown in supplemental Fig. S9.

January⁺¹–March⁺¹ on the duration of El Niño and La Niña by overlaying the magnitude of these factors on the scatterplots presented in Fig. 9. All of the factors appear to contribute to the diversity of the duration of late-onset El Niño and La Niña not preceded by a strong warm event. The overall correlations between the three indices and event duration (r_2) are significant at the 99% confidence level. These correlations, however, partly arise from the

correlations of the three indices to the onset timing and preceding event amplitude (r_1) (e.g., earlier onset of El Niño tends to lead to stronger positive IOD). Even after removing the dependency on the onset timing for El Niño and the preceding event amplitude for La Niña, the three indices are significantly correlated with the event duration (r_3). Thus, ocean–atmosphere variability outside the tropical Pacific modulates the event duration determined by the

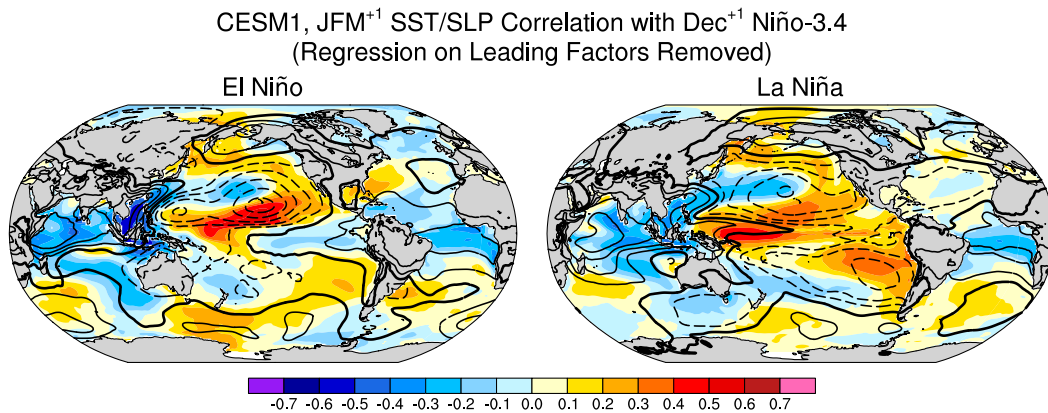


FIG. 11. Correlation maps of January⁺¹–March⁺¹ global surface temperature (shading) and SLP (contours at intervals of 0.1) anomalies with the December⁺¹ Niño-3.4 index for (left) El Niño and (right) La Niña events based on the CESM1 control simulation. Linear regressions on the onset month for El Niño and the December⁻¹ Niño-3.4 for La Niña are removed from the December⁺¹ Niño-3.4 index and surface temperature and SLP fields prior to the correlation analysis. The statistical significance of these anomalies is shown in supplemental Fig. S10.

ENSO dynamics and contributes to the diversity of the duration of individual events.

4. Summary and discussion

We have investigated the mechanisms controlling the duration of El Niño and La Niña events based on a suite of observational data and a long control simulation of CESM1. Our analyses show that the duration of El Niño and La Niña events is primarily determined by the onset timing and the amplitude of the preceding warm events, respectively. These factors affect the event duration through both oceanic and atmospheric processes as summarized in a schematic diagram in Fig. 14. Regarding the oceanic processes, an early onset of El Niño causes an early reflection of upwelling Rossby wave, effectively shoaling the thermocline in the eastern equatorial Pacific before the Bjerknes feedback strengthens in boreal summer following the mature phase. On the other hand, when a strong warm event precedes La Niña, the large discharge of the equatorial oceanic heat content requires more than one year for the equatorial Pacific to return to the neutral state. Regarding the atmospheric processes, an early onset of El Niño leads to fast adjustments of the tropical Atlantic and Indian Oceans to the tropical Pacific warming, weakening the positive interbasin SST gradient anomaly toward the Pacific. A strong warm event preceding La Niña, in contrast, causes not only strong cooling of the tropical Pacific but also delayed warming of the tropical Atlantic and Indian Oceans, strengthening the negative interbasin SST gradient anomaly toward the Pacific and delaying the adjustments of the Atlantic and Indian Oceans to the tropical Pacific cooling. For both El Niño and La Niña, the interbasin SST adjustments result

in weakening of surface wind anomalies over the western equatorial Pacific during winter–spring after the mature phase, which in turn act to reduce the thermocline depth anomalies in the eastern equatorial Pacific. Thus, both the oceanic and atmospheric adjustments are essential to the thermocline changes and hence the duration of El Niño and La Niña.

Most El Niño events that develop in boreal spring–early summer terminate after the mature phase, but El Niño events that develop in late summer–fall exhibit a large spread in their duration despite the overall tendency to last two years. Similarly, La Niña events preceded by a strong warm event usually last two years, but La Niña events following a moderate to weak El Niño show large variations in their duration. The duration spread unrelated to the onset timing for El Niño and the preceding event amplitude for La Niña is found to be related to ocean–atmosphere variability over the remote tropical oceans. In particular, variability of the IOD and equatorial Atlantic SSTs independent of the ENSO state affects the event duration by modulating the interbasin SST gradient when the duration is not strongly constrained by the tropical Pacific ocean–atmosphere state. In addition, stochastic variability of the NPO in winter–spring after the mature phase may also contribute to the diversity of event duration. Our diagnostic analysis and SST forcing used in the atmospheric model experiments are based on monthly data, and whether ocean–atmosphere processes on intraseasonal and shorter time scales are also important to the event duration still needs to be examined. For example, intraseasonal westerly wind events over the western Pacific warm pool have been suggested to affect the onset and development of El Niño events (e.g., Fedorov 2002;

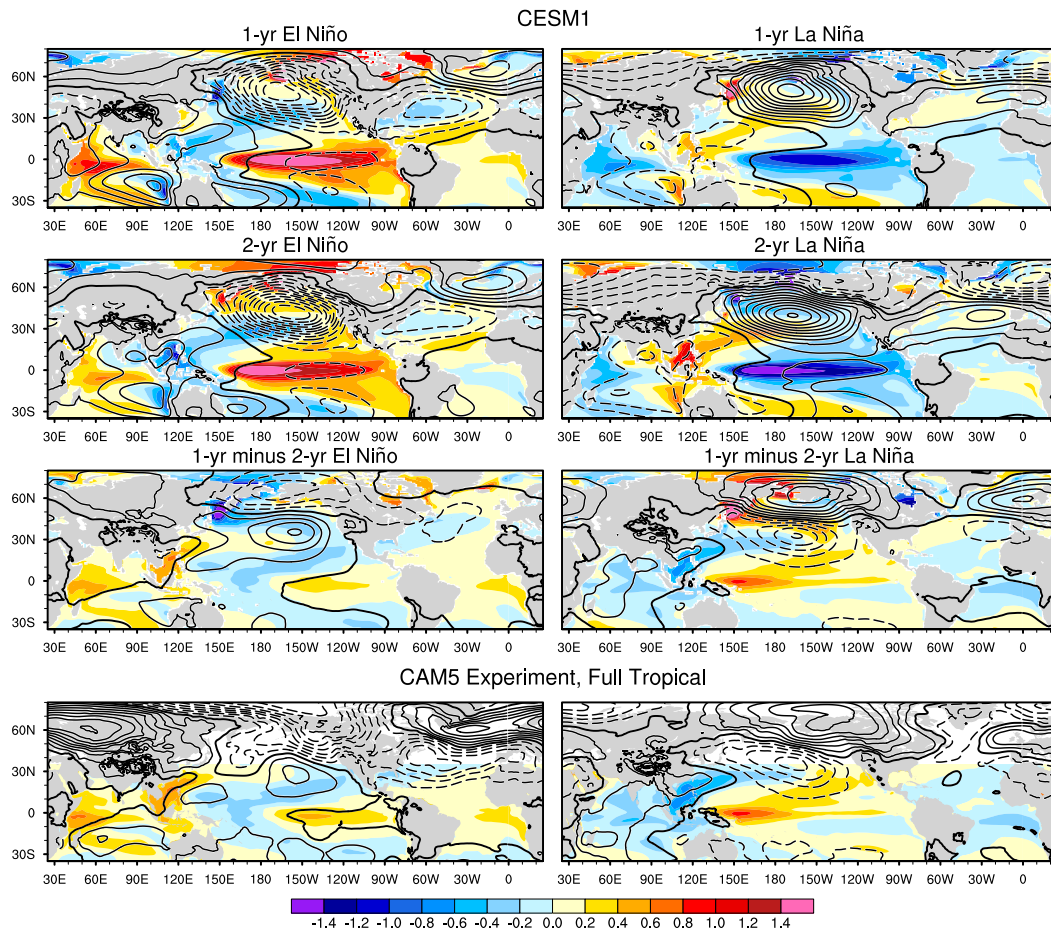


FIG. 12. Composite maps of January⁺¹–March⁺¹ SST (°C; shading) and SLP (contours at intervals of 0.6 hPa; zero contours thickened) anomalies for (top) 1- and (top middle) 2-yr (left) El Niño and (right) La Niña events based on the CESM1 control simulation. Also shown is the (bottom middle) difference between the top and top-middle rows. (bottom) As in the bottom-middle panels but based on the ensemble-mean response of the full tropical CAM5 experiment. The statistical significance of these anomalies is shown in supplemental Fig. S11.

Boulangier et al. 2004; Lengaigne et al. 2004; Puy et al. 2019), and they may also affect the temporal evolution of El Niño and La Niña events in the second year (Levine and McPhaden 2016; DiNezio et al. 2017a).

The frequent occurrence of 2-yr La Niña in recent several decades suggests that the duration of ENSO events may be modulated by interdecadal changes in tropical climate. Many previous studies show that the characteristics of ENSO exhibit low-frequency modulations in association with decadal–multidecadal climate variability in the Pacific (e.g., Rodgers et al. 2004; Yeh and Kirtman 2004; Choi et al. 2009; An and Choi 2015; Okumura et al. 2017a) and the Atlantic (e.g., Dong et al. 2006; Kang et al. 2014; Martín-Rey et al. 2014, 2015; Hu and Fedorov 2018), as well as with anthropogenic climate change (e.g., Timmermann et al. 1999; Collins et al. 2010; DiNezio et al. 2012; Kim et al. 2014; Cai et al. 2014). Most of these studies, however, focus on the

modulation of ENSO amplitude. A recent study by Okumura et al. (2017a) shows that the duration of ENSO events also varies closely with the leading modes of tropical Pacific decadal variability through diagnostic analyses of a CCSM4 control simulation. In this model, the duration of El Niño is affected by decadal changes in the interbasin SST gradient while the duration of La Niña is controlled more by decadal changes in the ENSO amplitude. Ohba (2013) also suggests that the duration of El Niño is modulated by decadal changes in the Indo-Pacific interbasin coupling. Further studies are needed to understand how the ENSO event duration is affected by decadal variability in the tropical oceans, as well as their interbasin coupling.

Our diagnostic analyses of the mechanisms controlling the duration of El Niño and La Niña could serve as a basis for the predictions of ENSO event duration. The

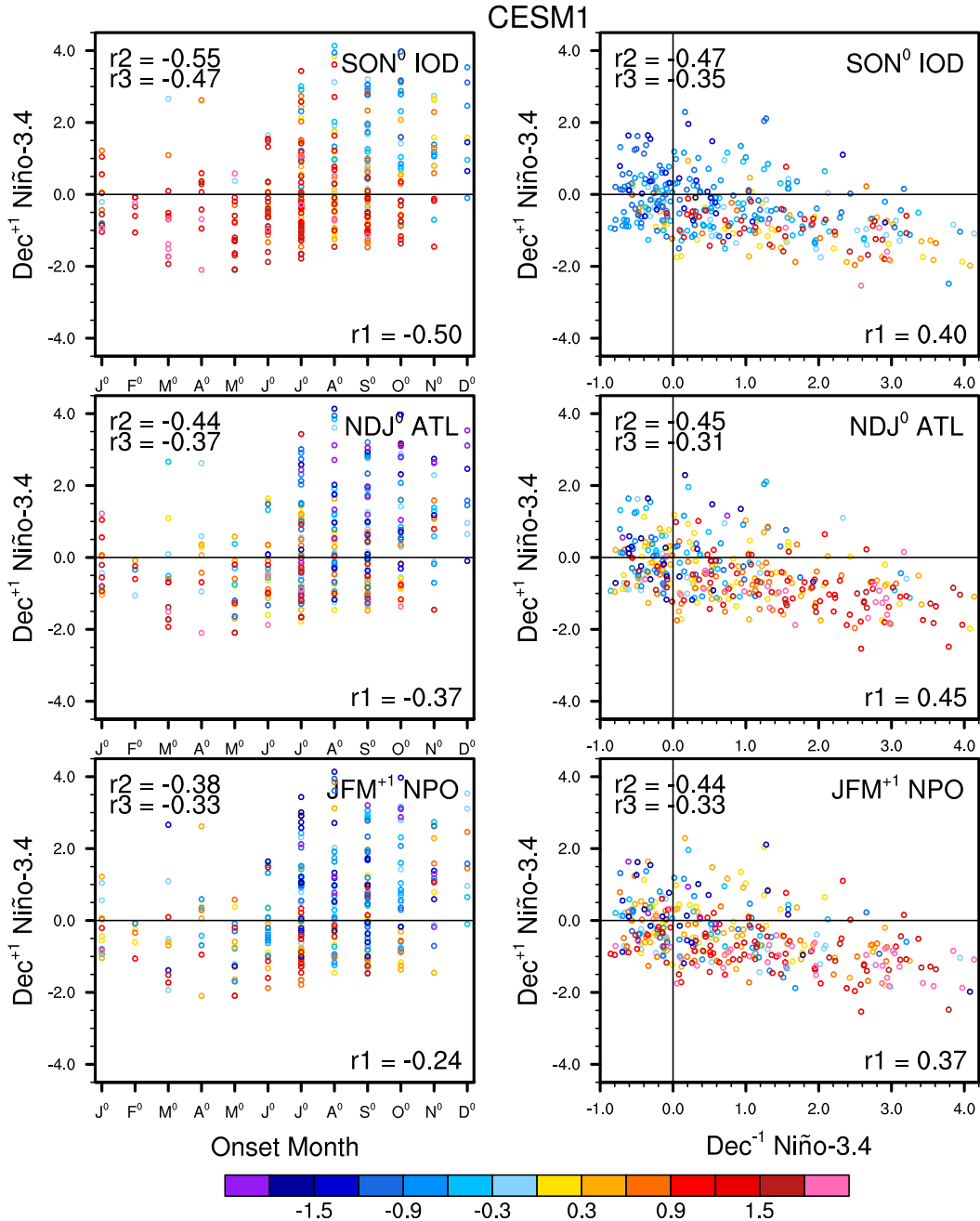


FIG. 13. Scatterplots of the December⁺¹ Niño-3.4 index (°C) vs (left) the onset month for El Niño events and (right) the December⁻¹ Niño-3.4 index for La Niña events. The colors of circles represent the values of the standardized (top) IOD index in September⁰–November⁰ (10°S–10°N, 50°–70°E minus 10°S–0°, 90°–100°E), (middle) equatorial Atlantic SST index in November⁰–January⁺¹ (3°S–3°N, 50°W–0°), and (bottom) NPO index in January⁺¹–March⁺¹ [the second leading principal component of SLP variability over the North Pacific (15°–70°N, 130°E–110°W)]. The correlation coefficients of the indices shown in colors with the horizontal coordinate values (r_1) are indicated at the bottom-right corner of each panel. The correlation coefficients of the indices shown in colors with the vertical coordinate values (r_2) and those after removing the linear regressions on the horizontal coordinate values (r_3) are indicated at the top-left corner of each plot.

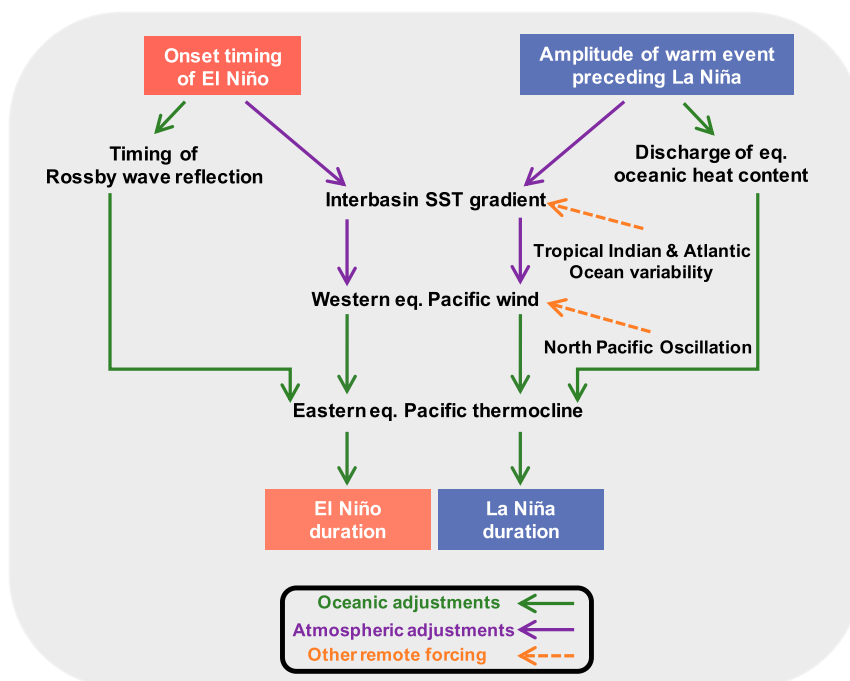


FIG. 14. Schematic diagram illustrating the oceanic and atmospheric processes by which the duration of El Niño and La Niña is affected by the onset timing and the amplitude of the preceding warm event, respectively. The adjustment processes primarily through the ocean or atmosphere are indicated by green or purple arrows, respectively, and the processes external to the ENSO dynamics are indicated by yellow arrows.

early precursors suggest potential predictability of ENSO event duration with a long lead time. Nevertheless, the current operational ENSO forecasts are limited to approximately 8 months (Barnston et al. 2012), precluding the prediction of multiyear ENSO events. Recent studies have successfully predicted the return of La Niña events in the second year with a 2-yr lead time (DiNezio et al. 2017a,b; Luo et al. 2008, 2017). Further studies are in progress to understand the predictability of the duration of both El Niño and La Niña events.

Acknowledgments. The authors thank Drs. Shang-Ping Xie, Clara Deser, Axel Timmermann, and David Battisti for helpful discussions. Comments and suggestions by three anonymous reviewers helped to improve the paper. The CESM1 and CAM5 control simulations are conducted by the CESM project team and are available via the Earth System Grid. The observational datasets used in this study are obtained online: HadISST from the Met Office Hadley Center (<http://www.metoffice.gov.uk/hadobs/>), 20CR from the NOAA Earth System Research Laboratory Physical Science Division (<https://www.esrl.noaa.gov/psd/>), and the SODA analysis from the Asia-Pacific Data Research Center (<http://apdrc.soest.hawaii.edu/>). The study is supported by the NOAA Climate Program Office

Modeling, Analysis, Predictions, and Projections Program (NA17OAR4310149 and NA17OAR4310145) and the NSF Climate and Large-Scale Dynamics Program (OCN-1756883).

REFERENCES

- Alexander, M. A., I. Blade, M. Newman, J. R. Lanzante, N.-C. Lau, and J. D. Scott, 2002: The atmospheric bridge: The influence of ENSO teleconnections on air–sea interaction over the global oceans. *J. Climate*, **15**, 2205–2231, [https://doi.org/10.1175/1520-0442\(2002\)015<2205:TABTIO>2.0.CO;2](https://doi.org/10.1175/1520-0442(2002)015<2205:TABTIO>2.0.CO;2).
- , D. J. Vimont, P. Chang, and J. D. Scott, 2010: The impact of extratropical atmospheric variability on ENSO: Testing the seasonal footprinting mechanism using coupled model experiments. *J. Climate*, **23**, 2885–2901, <https://doi.org/10.1175/2010JCLI3205.1>.
- An, S.-I., and J. Choi, 2015: Why the twenty-first century tropical Pacific trend pattern cannot significantly influence ENSO amplitude? *Climate Dyn.*, **44**, 133–146, <https://doi.org/10.1007/s00382-014-2233-2>.
- , and J.-W. Kim, 2017: Role of nonlinear ocean dynamic response to wind on the asymmetrical transition of El Niño and La Niña. *Geophys. Res. Lett.*, **44**, 393–400, <https://doi.org/10.1002/2016GL071971>.
- , and —, 2018: ENSO transition asymmetry: Internal and external causes and intermodel diversity. *Geophys. Res. Lett.*, **45**, 5095–5104, <https://doi.org/10.1029/2018GL078476>.

- Anderson, B. T., 2003: Tropical Pacific sea-surface temperatures and preceding sea level pressure anomalies in the subtropical North Pacific. *J. Geophys. Res.*, **108**, 4732, <https://doi.org/10.1029/2003JD003805>.
- Annamalai, H., S.-P. Xie, J. P. McCreary, and R. Murtugudde, 2005: Impact of Indian Ocean sea surface temperature on developing El Niño. *J. Climate*, **18**, 302–319, <https://doi.org/10.1175/JCLI-3268.1>.
- Barnston, A. G., M. K. Tippett, M. L. L'Heureux, S. Li, and D. G. DeWitt, 2012: Skill of real-time seasonal ENSO model predictions during 2002–11: Is our capability increasing? *Bull. Amer. Meteor. Soc.*, **93**, 631–651, <https://doi.org/10.1175/BAMS-D-11-00111.1>.
- Battisti, D. S., and A. C. Hirst, 1989: Interannual variability in a tropical atmosphere–ocean model: Influence of the basic state, ocean geometry and nonlinearity. *J. Atmos. Sci.*, **46**, 1687–1712, [https://doi.org/10.1175/1520-0469\(1989\)046<1687:IVIATA>2.0.CO;2](https://doi.org/10.1175/1520-0469(1989)046<1687:IVIATA>2.0.CO;2).
- Bjerknes, J., 1969: Atmospheric teleconnections from the equatorial Pacific. *Mon. Wea. Rev.*, **97**, 163–172, [https://doi.org/10.1175/1520-0493\(1969\)097<0163:ATFTEP>2.3.CO;2](https://doi.org/10.1175/1520-0493(1969)097<0163:ATFTEP>2.3.CO;2).
- Boulanger, J.-P., C. Menkes, and M. Lengaigne, 2004: Role of high- and low-frequency winds and wave reflection in the onset, growth and termination of the 1997–1998 El Niño. *Climate Dyn.*, **22**, 267–280, <https://doi.org/10.1007/s00382-003-0383-8>.
- Burgers, G., and D. B. Stephenson, 1999: The “normality” of El Niño. *Geophys. Res. Lett.*, **26**, 1027–1039, <https://doi.org/10.1029/1999GL900161>.
- Cai, W., and Coauthors, 2014: Increasing frequency of extreme El Niño events due to greenhouse warming. *Nat. Climate Change*, **4**, 111–116, <https://doi.org/10.1038/nclimate2100>.
- , and Coauthors, 2019: Pantropical climate interactions. *Science*, **363**, eaav4236, <https://doi.org/10.1126/science.aav4236>.
- Carton, J. A., and B. S. Giese, 2008: A reanalysis of ocean climate using Simple Ocean Data Assimilation (SODA). *Mon. Wea. Rev.*, **136**, 2999–3017, <https://doi.org/10.1175/2007MWR1978.1>.
- Chang, P., and Coauthors, 2006: Climate fluctuations of tropical coupled systems—The role of ocean dynamics. *J. Climate*, **19**, 5122–5174, <https://doi.org/10.1175/JCLI3903.1>.
- , L. Zhang, R. Saravanan, D. J. Vimont, J. C. H. Chiang, L. Ji, H. Seidel, and M. K. Tippett, 2007: Pacific meridional mode and El Niño–Southern Oscillation. *Geophys. Res. Lett.*, **34**, L16608, <https://doi.org/10.1029/2007GL030302>.
- Chen, M.-C., T. Li, X.-Y. Shen, and B. Wu, 2016: Relative roles of dynamic and thermodynamic processes in causing evolution asymmetry between El Niño and La Niña. *J. Climate*, **29**, 2201–2220, <https://doi.org/10.1175/JCLI-D-15-0547.1>.
- Choi, J., S.-I. An, B. Dewitte, and W. W. Hsieh, 2009: Interactive feedback between the tropical Pacific decadal oscillation and ENSO in a coupled general circulation model. *J. Climate*, **22**, 6597–6611, <https://doi.org/10.1175/2009JCLI2782.1>.
- Choi, K.-Y., G. A. Vecchi, and A. T. Wittenberg, 2013: ENSO transition, duration, and amplitude asymmetries: Role of the nonlinear wind stress coupling in a conceptual model. *J. Climate*, **26**, 9462–9476, <https://doi.org/10.1175/JCLI-D-13-00045.1>.
- Collins, M., and Coauthors, 2010: The impact of global warming on the tropical Pacific and El Niño. *Nat. Geosci.*, **3**, 391–397, <https://doi.org/10.1038/ngeo868>.
- Compo, G. P., and Coauthors, 2011: The Twentieth Century Reanalysis Project. *Quart. J. Roy. Meteor. Soc.*, **137**, 1–28, <https://doi.org/10.1002/qj.776>.
- Deser, C., and Coauthors, 2012: ENSO and Pacific decadal variability in the Community Climate System Model version 4. *J. Climate*, **25**, 2622–2651, <https://doi.org/10.1175/JCLI-D-11-00301.1>.
- DiNezio, P. N., and C. Deser, 2014: Nonlinear controls on the persistence of La Niña. *J. Climate*, **27**, 7335–7355, <https://doi.org/10.1175/JCLI-D-14-00033.1>.
- , B. P. Kirtman, A. C. Clement, S.-K. Lee, G. A. Vecchi, and A. Wittenberg, 2012: Mean climate controls on the simulated response of ENSO to increasing greenhouse gases. *J. Climate*, **25**, 7399–7420, <https://doi.org/10.1175/JCLI-D-11-00494.1>.
- , C. Deser, Y. M. Okumura, and A. Karspeck, 2017a: Predictability of 2-year La Niña events in a coupled general circulation model. *Climate Dyn.*, **49**, 4237–4261, <https://doi.org/10.1007/S00382-017-3575-3>.
- , and Coauthors, 2017b: A 2 year forecast for a 60–80% chance of La Niña in 2017–2018. *Geophys. Res. Lett.*, **44**, 11 624–11 635, <https://doi.org/10.1002/2017GL074904>.
- Ding, H., N. S. Keenlyside, and M. Latif, 2012: Impact of the equatorial Atlantic on the El Niño Southern Oscillation. *Climate Dyn.*, **38**, 1965–1972, <https://doi.org/10.1007/s00382-011-1097-y>.
- Dommenges, D., T. Bayr, and C. Frauen, 2013: Analysis of the nonlinearity in the pattern and time evolution of El Niño southern oscillation. *Climate Dyn.*, **40**, 2825–2847, <https://doi.org/10.1007/s00382-012-1475-0>.
- Dong, B., R. T. Sutton, and A. A. Scaife, 2006: Multidecadal modulation of El Niño–Southern Oscillation (ENSO) variance by Atlantic Ocean sea surface temperatures. *Geophys. Res. Lett.*, **33**, L08705, <https://doi.org/10.1029/2006GL025766>.
- Fedorov, A. V., 2002: The response of the coupled tropical ocean–atmosphere to westerly wind bursts. *Quart. J. Roy. Meteor. Soc.*, **128**, 1–23, <https://doi.org/10.1002/qj.200212857901>.
- Gadgil, S., P. V. Joseph, and N. V. Joshi, 1984: Ocean–atmosphere coupling over monsoon regions. *Nature*, **312**, 141–143, <https://doi.org/10.1038/312141a0>.
- Gent, P. R., and Coauthors, 2011: The Community Climate System Model version 4. *J. Climate*, **24**, 4973–4991, <https://doi.org/10.1175/2011JCLI4083.1>.
- Graham, N. E., and T. P. Barnett, 1987: Sea surface temperature, surface wind divergence, and convection over tropical oceans. *Science*, **238**, 657–659, <https://doi.org/10.1126/science.238.4827.657>.
- Ham, Y.-G., and J.-S. Kug, 2015: Role of north tropical Atlantic SST on the ENSO simulated using CMIP3 and CMIP5 models. *Climate Dyn.*, **45**, 3103–3117, <https://doi.org/10.1007/s00382-015-2527-z>.
- Harrison, D. E., and G. A. Vecchi, 1999: On the termination of El Niño. *Geophys. Res. Lett.*, **26**, 1593–1596, <https://doi.org/10.1029/1999GL900316>.
- Hoerling, M. P., and A. Kumar, 2003: The perfect ocean for drought. *Science*, **299**, 691–694, <https://doi.org/10.1126/science.1079053>.
- , —, and M. Zhong, 1997: El Niño, La Niña, and the nonlinearity of their teleconnections. *J. Climate*, **10**, 1769–1786, [https://doi.org/10.1175/1520-0442\(1997\)010<1769:ENOLNA>2.0.CO;2](https://doi.org/10.1175/1520-0442(1997)010<1769:ENOLNA>2.0.CO;2).
- , and Coauthors, 2013: Anatomy of an extreme event. *J. Climate*, **26**, 2811–2832, <https://doi.org/10.1175/JCLI-D-12-00270.1>.
- Hong, C.-C., T. Li, LinHo, and Y.-C. Chen, 2010: Asymmetry of the Indian Ocean basinwide SST anomalies: Roles of ENSO and IOD. *J. Climate*, **23**, 3563–3576, <https://doi.org/10.1175/2010JCLI3320.1>.
- Horii, T., and K. Hanawa, 2004: A relationship between timing of El Niño onset and subsequent evolution. *Geophys. Res. Lett.*, **31**, L06304, <https://doi.org/10.1029/2003GL019239>.

- Hu, S., and A. V. Fedorov, 2018: Cross-equatorial winds control El Niño diversity and change. *Nat. Climate Change*, **8**, 798, <https://doi.org/10.1038/s41558-018-0248-0>.
- Hu, Z.-Z., A. Kumar, Y. Xue, and B. Jha, 2014: Why were some La Niñas followed by another La Niña? *Climate Dyn.*, **42**, 1029–1042, <https://doi.org/10.1007/s00382-013-1917-3>.
- Hurrell, J., and Coauthors, 2013: The Community Earth System Model: A framework for collaborative research. *Bull. Amer. Meteor. Soc.*, **94**, 1339–1360, <https://doi.org/10.1175/BAMS-D-12-00121.1>.
- Izumo, T., and Coauthors, 2010: Influence of the state of the Indian Ocean dipole on the following year's El Niño. *Nat. Geosci.*, **3**, 168–172, <https://doi.org/10.1038/ngeo760>.
- Jansen, M. F., D. Dommenget, and N. Keenlyside, 2009: Tropical atmosphere–ocean interactions in a conceptual framework. *J. Climate*, **22**, 550–567, <https://doi.org/10.1175/2008JCLI2243.1>.
- Jin, F.-F., 1997: An equatorial ocean recharge paradigm for ENSO. Part I: Conceptual model. *J. Atmos. Sci.*, **54**, 811–829, [https://doi.org/10.1175/1520-0469\(1997\)054<0811:AEORPF>2.0.CO;2](https://doi.org/10.1175/1520-0469(1997)054<0811:AEORPF>2.0.CO;2).
- Kang, I.-S., H.-H. No, and F. Kucharski, 2014: ENSO amplitude modulation associated with the mean SST changes in the tropical central Pacific induced by Atlantic multidecadal oscillation. *J. Climate*, **27**, 7911–7920, <https://doi.org/10.1175/JCLI-D-14-00018.1>.
- Kay, J. E., and Coauthors, 2015: The Community Earth System Model (CESM) Large Ensemble Project: A community resource for studying climate change in the presence of internal climate variability. *Bull. Amer. Meteor. Soc.*, **96**, 1333–1349, <https://doi.org/10.1175/BAMS-D-13-00255.1>.
- Keenlyside, N. S., H. Ding, and M. Latif, 2013: Potential of equatorial Atlantic variability to enhance El Niño prediction. *Geophys. Res. Lett.*, **40**, 2278–2283, <https://doi.org/10.1002/grl.50362>.
- Kessler, W. S., 2002: Is ENSO a cycle or a series of events? *Geophys. Res. Lett.*, **29**, 2125, <https://doi.org/10.1029/2002GL015924>.
- Kim, S. T., W. Cai, F.-F. Jin, A. Santoso, L. Wu, E. Guilyardi, and S.-I. An, 2014: Response of El Niño sea surface temperature variability to greenhouse warming. *Nat. Climate Change*, **4**, 786–790, <https://doi.org/10.1038/nclimate2326>.
- Kirtman, B. P., 1997: Oceanic Rossby wave dynamics and the ENSO period in a coupled model. *J. Climate*, **10**, 1690–1704, [https://doi.org/10.1175/1520-0442\(1997\)010<1690:ORWDAT>2.0.CO;2](https://doi.org/10.1175/1520-0442(1997)010<1690:ORWDAT>2.0.CO;2).
- Kug, J.-S., and I.-S. Kang, 2006: Interactive feedback between ENSO and the Indian Ocean. *J. Climate*, **19**, 1784–1801, <https://doi.org/10.1175/JCLI3660.1>.
- Larkin, N. K., and D. E. Harrison, 2002: ENSO warm (El Niño) and cold (La Niña) event life cycles: Ocean surface anomaly patterns, their symmetries, asymmetries, and implications. *J. Climate*, **15**, 1118–1140, [https://doi.org/10.1175/1520-0442\(2002\)015<1118:EWENOA>2.0.CO;2](https://doi.org/10.1175/1520-0442(2002)015<1118:EWENOA>2.0.CO;2).
- Lee, S.-K., P. N. DiNezio, E.-S. Chung, S.-W. Yeh, A. T. Wittenberg, and C. Wang, 2014: Spring persistence, transition and resurgence of El Niño. *Geophys. Res. Lett.*, **41**, 8578–8585, <https://doi.org/10.1002/2014GL062484>.
- Lengaigne, M., E. Guilyardi, J.-P. Boulanger, C. Menkes, P. Delecluse, P. Inness, J. Cole, and J. M. Slingo, 2004: Triggering of El Niño by westerly wind events in a coupled general circulation model. *Climate Dyn.*, **23**, 601–620, <https://doi.org/10.1007/s00382-004-0457-2>.
- Levine, A. F. Z., and M. J. McPhaden, 2016: How the July 2014 easterly wind burst gave the 2015–2016 El Niño a head start. *Geophys. Res. Lett.*, **43**, 6503–6510, <https://doi.org/10.1002/2016GL069204>.
- Li, X., S.-P. Xie, S. T. Gille, and C. Yoo, 2016: Atlantic-induced pan-tropical climate change over the past three decades. *Nat. Climate Change*, **6**, 275–279, <https://doi.org/10.1038/nclimate2840>.
- Luo, J.-J., S. Masson, S. K. Behera, and T. Yamagata, 2008: Extended ENSO predictions using a fully coupled ocean–atmosphere model. *J. Climate*, **18**, 2344–2360, <https://doi.org/10.1175/2007JCLI1412.1>.
- , G. Liu, H. Hendon, O. Alves, and T. Yamagata, 2017: Interbasin sources for two-year predictability of the multi-year La Niña event in 2010–2012. *Sci. Rep.*, **7**, 2276, <https://doi.org/10.1038/s41598-017-01479-9>.
- Martín-Rey, M., B. Rodríguez-Fonseca, I. Polo, and F. Kucharski, 2014: On the Atlantic–Pacific Niños connection: A multi-decadal modulated mode. *Climate Dyn.*, **43**, 3163–3178, <https://doi.org/10.1007/s00382-014-2305-3>.
- , —, and —, 2015: Atlantic opportunities for ENSO prediction. *Geophys. Res. Lett.*, **42**, 6802–6810, <https://doi.org/10.1002/2015GL065062>.
- McGregor, S., A. Timmermann, N. Schneider, M. F. Stuecker, and M. H. England, 2012: The effect of the South Pacific convergence zone on the termination of El Niño events and the meridional asymmetry of ENSO. *J. Climate*, **25**, 5566–5586, <https://doi.org/10.1175/JCLI-D-11-00332.1>.
- , N. Ramesh, P. Spence, M. H. England, M. J. McPhaden, and A. Santoso, 2013: Meridional movement of wind anomalies during ENSO events and their role in event termination. *Geophys. Res. Lett.*, **40**, 749–754, <https://doi.org/10.1002/grl.50136>.
- , A. Timmermann, M. F. Stuecker, M. H. England, M. Merrifield, F.-F. Jin, and Y. Chikamoto, 2014: Recent Walker circulation strengthening and Pacific cooling amplified by Atlantic warming. *Nat. Climate Change*, **4**, 888–892, <https://doi.org/10.1038/nclimate2330>.
- McPhaden, M. J., and X. Zhang, 2009: Asymmetry in zonal phase propagation of ENSO sea surface temperature anomalies. *Geophys. Res. Lett.*, **36**, L13703, <https://doi.org/10.1029/2009GL038774>.
- Meinen, C. S., and M. J. McPhaden, 2000: Observations of warm water volume changes in the equatorial Pacific and their relationship to El Niño and La Niña. *J. Climate*, **13**, 3551–3559, [https://doi.org/10.1175/1520-0442\(2000\)013<3551:OOWWVC>2.0.CO;2](https://doi.org/10.1175/1520-0442(2000)013<3551:OOWWVC>2.0.CO;2).
- Mitchell, T. P., and J. M. Wallace, 1992: The annual cycle in equatorial convection and sea surface temperature. *J. Climate*, **5**, 1140–1156, [https://doi.org/10.1175/1520-0442\(1992\)005<1140:TACIEC>2.0.CO;2](https://doi.org/10.1175/1520-0442(1992)005<1140:TACIEC>2.0.CO;2).
- Nagura, M., and M. Konda, 2007: The seasonal development of an SST anomaly in the Indian Ocean and its relationship to ENSO. *J. Climate*, **20**, 38–52, <https://doi.org/10.1175/JCLI3986.1>.
- Neale, R. B., and Coauthors, 2012: Description of the NCAR Community Atmosphere Model (CAM 5.0). NCAR Tech. Note NCAR/TN-486+STR, 274 pp., www.cesm.ucar.edu/models/cesm1.0/cam/docs/description/cam5_desc.pdf.
- Neelin, J. D., D. S. Battisti, A. C. Hirst, F.-F. Jin, Y. Wakata, T. Yamagata, and S. E. Zebiak, 1998: ENSO theory. *J. Geophys. Res.*, **103**, 14 261–14 290, <https://doi.org/10.1029/97JC03424>.
- Ohba, M., 2013: Important factors for long-term change in ENSO transitivity. *Int. J. Climatol.*, **33**, 1495–1509, <https://doi.org/10.1002/joc.3529>.
- , and H. Ueda, 2007: An impact of SST anomalies in the Indian Ocean in acceleration of the El Niño to La Niña transition. *J. Meteor. Soc. Japan*, **85**, 335–348, <https://doi.org/10.2151/jmsj.85.335>.

- , and —, 2009: Role of nonlinear atmospheric response to SST on the asymmetric transition process of ENSO. *J. Climate*, **22**, 177–192, <https://doi.org/10.1175/2008JCLI2334.1>.
- , and M. Watanabe, 2012: Role of the Indo-Pacific interbasin coupling in predicting asymmetric ENSO transition and duration. *J. Climate*, **25**, 3321–3335, <https://doi.org/10.1175/JCLI-D-11-00409.1>.
- Okumura, Y. M., and C. Deser, 2010: Asymmetry in the duration of El Niño and La Niña. *J. Climate*, **23**, 5826–5843, <https://doi.org/10.1175/2010JCLI3592.1>.
- , M. Ohba, C. Deser, and H. Ueda, 2011: A proposed mechanism for the asymmetric duration of El Niño and La Niña. *J. Climate*, **24**, 3822–3829, <https://doi.org/10.1175/2011JCLI9999.1>.
- , T. Sun, and X. Wu, 2017a: Asymmetric modulation of El Niño and La Niña and the linkage to tropical Pacific decadal variability. *J. Climate*, **30**, 4705–4733, <https://doi.org/10.1175/JCLI-D-16-0680.1>.
- , P. N. DiNezio, and C. Deser, 2017b: Evolving impacts of multiyear La Niña Events on atmospheric circulation and U.S. drought. *Geophys. Res. Lett.*, **44**, 11 614–11 623, <https://doi.org/10.1002/2017GL075034>.
- Polo, I., M. Martin-Rey, B. Rodríguez-Fonseca, F. Kucharski, and C. R. Mechoso, 2015: Processes in the Pacific La Niña onset triggered by the Atlantic Niño. *Climate Dyn.*, **44**, 115–131, <https://doi.org/10.1007/s00382-014-2354-7>.
- Puy, M., and Coauthors, 2019: Influence of westerly wind events stochasticity on El Niño amplitude: The case of 2014 vs. 2015. *Climate Dyn.*, **52**, 7435–7454, <https://doi.org/10.1007/S00382-017-3938-9>.
- Rayner, N. A., D. E. Parker, E. B. Horton, C. K. Folland, L. Alexandre, D. P. Rowell, E. C. Kent, and A. Kaplan, 2003: Global analyses of sea surface temperature, sea ice, and night marine air temperature since the late nineteenth century. *J. Geophys. Res.*, **108**, 4407, <https://doi.org/10.1029/2002JD002670>.
- Rodgers, K. B., P. Friederichs, and M. Latif, 2004: Tropical Pacific decadal variability and its relation to decadal modulations of ENSO. *J. Climate*, **17**, 3761–3774, [https://doi.org/10.1175/1520-0442\(2004\)017<3761:TPDVAI>2.0.CO;2](https://doi.org/10.1175/1520-0442(2004)017<3761:TPDVAI>2.0.CO;2).
- Rodríguez-Fonseca, B., I. Polo, J. García-Serrano, T. Losada, E. Mohino, C. R. Mechoso, and F. Kucharski, 2009: Are Atlantic Niños enhancing Pacific ENSO events in recent decades? *Geophys. Res. Lett.*, **36**, L20705, <https://doi.org/10.1029/2009GL040048>.
- Schneider, E. K., B. Huang, and J. Shukla, 1995: Ocean wave dynamics and El Niño. *J. Climate*, **8**, 2415–2439, [https://doi.org/10.1175/1520-0442\(1995\)008<2415:OWDAEN>2.0.CO;2](https://doi.org/10.1175/1520-0442(1995)008<2415:OWDAEN>2.0.CO;2).
- Schott, F. A., S.-P. Xie, and J. P. McCreary, 2009: Indian Ocean circulation and climate variability. *Rev. Geophys.*, **47**, RG1002, <https://doi.org/10.1029/2007RG000245>.
- Schubert, S. D., and Coauthors, 2016: Global meteorological drought: A synthesis of current understanding with a focus on SST drivers of precipitation deficits. *J. Climate*, **29**, 3989–4019, <https://doi.org/10.1175/JCLI-D-15-0452.1>.
- Seager, R., and M. Hoerling, 2014: Atmosphere and ocean origins of North American droughts. *J. Climate*, **27**, 4581–4606, <https://doi.org/10.1175/JCLI-D-13-00329.1>.
- Stein, K., A. Timmermann, F.-F. Jin, and M. F. Stuecker, 2014: ENSO seasonal synchronization theory. *J. Climate*, **27**, 5285–5310, <https://doi.org/10.1175/JCLI-D-13-00525.1>.
- Suarez, M. J., and P. S. Schopf, 1988: A delayed action oscillator for ENSO. *J. Atmos. Sci.*, **45**, 3283–3287, [https://doi.org/10.1175/1520-0469\(1988\)045<3283:ADAOFE>2.0.CO;2](https://doi.org/10.1175/1520-0469(1988)045<3283:ADAOFE>2.0.CO;2).
- Timmermann, A., J. Oberhuber, A. Bacher, M. Esch, and M. Latif, 1999: Increased El Niño frequency in a climate model by future greenhouse warming. *Nature*, **398**, 694–696, <https://doi.org/10.1038/19505>.
- Trenberth, K. E., G. W. Branstator, D. Karoly, A. Kumar, N.-C. Lau, and C. Ropelewski, 1998: Progress during TOGA in understanding and modeling global teleconnections associated with tropical sea surface temperatures. *J. Geophys. Res.*, **103**, 14 291–14 324, <https://doi.org/10.1029/97JC01444>.
- Vecchi, G. A., 2006: The termination of the 1997/98 El Niño. Part II: Mechanisms of atmospheric change. *J. Climate*, **19**, 2647–2664, <https://doi.org/10.1175/JCLI3780.1>.
- Vimont, D. J., D. S. Battisti, and A. C. Hirst, 2001: Footprinting: A seasonal connection between the tropics and mid-latitudes. *Geophys. Res. Lett.*, **28**, 3923–3926, <https://doi.org/10.1029/2001GL013435>.
- , J. M. Wallace, and D. S. Battisti, 2003: The seasonal footprinting mechanism in the Pacific: Implications for ENSO. *J. Climate*, **16**, 2668–2675, [https://doi.org/10.1175/1520-0442\(2003\)016<2668:TSFMIT>2.0.CO;2](https://doi.org/10.1175/1520-0442(2003)016<2668:TSFMIT>2.0.CO;2).
- Wallace, J. M., E. M. Rasmusson, T. P. Mitchell, V. E. Koussy, E. S. Sarachik, and H. von Storch, 1998: On the structure and evolution of ENSO-related climate variability in the tropical Pacific: Lessons from TOGA. *J. Geophys. Res.*, **103**, 14 241–14 259, <https://doi.org/10.1029/97JC02905>.
- Wang, C., 2006: An overlooked feature of tropical climate: Inter-Pacific-Atlantic variability. *Geophys. Res. Lett.*, **33**, L12702, <https://doi.org/10.1029/2006GL026324>.
- , and J. Picaut, 2004: Understanding ENSO physics—A review. *Earth's Climate: The Ocean–Atmosphere Interaction, Geophys. Monogr.*, Vol. 147, Amer. Geophys. Union, 21–48.
- Wang, L., J.-Y. Yu, and H. Paek, 2017: Enhanced biennial variability in the Pacific due to Atlantic capacitor effect. *Nat. Commun.*, **8**, 14 887, <https://doi.org/10.1038/ncomms14887>.
- Weisberg, R. H., and C. Wang, 1997: A western Pacific oscillator paradigm for the El Niño–Southern Oscillation. *Geophys. Res. Lett.*, **24**, 779–782, <https://doi.org/10.1029/97GL00689>.
- Wu, B., T. Li, and T. Zhou, 2010: Asymmetry of atmospheric circulation anomalies over the western North Pacific between El Niño and La Niña. *J. Climate*, **23**, 4807–4822, <https://doi.org/10.1175/2010JCLI3222.1>.
- Xie, S.-P., and J. A. Carton, 2004: Tropical Atlantic variability: Patterns, mechanisms, and impacts. *Earth's Climate: The Ocean–Atmosphere Interaction, Geophys. Monogr.*, Vol. 147, Amer. Geophys. Union, 121–142.
- Yeh, S.-W., and B. P. Kirtman, 2004: Tropical Pacific decadal variability and ENSO amplitude modulation in a CGCM. *J. Geophys. Res.*, **109**, C11009, <https://doi.org/10.1029/2004JC002442>.
- Yoo, S.-H., J. Fasullo, S. Yang, and C.-H. Ho, 2010: On the relationship between Indian Ocean sea surface temperature and the transition from El Niño to La Niña. *J. Geophys. Res.*, **115**, D15114, <https://doi.org/10.1029/2009JD012978>.